Geological Society of America
Special Paper 409
2006

Timing and nature of postcollisional volcanism in western Anatolia and geodynamic implications

Şafak Altunkaynak*
Department of Geological Engineering, Istanbul Technical University, Maslak 80626, Istanbul, Turkey
Yildirim Dilek
Department of Geology, Miami University, Oxford, Ohio 45056, USA

ABSTRACT

Western Anatolia (Turkey) has experienced discrete pulses of widespread volcanism since the collision of the Sakarya and Tauride continental blocks in the early Eocene. Underplating of the leading edge of the Tauride platform at a north-dipping subduction zone beneath the Sakarya continent resulted in crustal thickening and detachment of the Neo-Tethyan oceanic lithosphere from continental lithosphere, causing slab break-off and the development of an asthenospheric window. Thermal perturbation caused by this asthenospheric upwelling led to melting of the metasomatized overriding mantle lithosphere that produced volcanism and granitic plutonism across the suture zone and the Sakarya continent. The products of this first episode of postcollisional volcanism in western Anatolia were subalkaline in character, with rocks ranging in composition from basalt, basaltic andesite, and andesite to dacite; they show enrichment in large-ion lithophile elements (LILE) and light rare earth elements (LREE) relative to the high field strength elements and display the highest $^{87}Sr/^{86}Sr$ (i) (0.7087 to 0.7071) and the lowest εNd (i) (–6.5 to –3.5) values in comparison to the rocks of the following volcanic episodes. Geochemical features and compositional variations of this subalkaline volcanic group indicate increasing amounts of crustal contamination and a decreasing subduction signature during their evolution from the Eocene through the Oligo-Miocene.

Following the initial phases of orogenic collapse, collision-induced compression in western Anatolia was replaced by north-south extension in the early to middle Miocene that produced metamorphic core complexes and NNE-trending horst-graben structures in the region. The second major volcanic episode from 16 to 14 Ma produced mildly alkaline rocks ranging in composition from basalt, trachy-basalt, and trachyandesite to trachyte, showing enrichment in LILE and LREE (although less pronounced in comparison to the subalkaline lavas), with $^{87}Sr/^{86}Sr$ (i) (0.7075 to 0.7062) and εNd (i) (–3.6 to –1.6) values that are transitional between the earlier subalkaline and the later alkaline group lavas. Melting of a subduction-modified lithospheric mantle and asthenospheric melts appear to have contributed to the magma budget of the mildly alkaline group, which shows the effects of less crustal contamination or assimilation as a result of advanced crustal thinning associated with tectonic extension

*E-mail: safak@itu.edu.tr.

Altunkaynak, Ş., and Dilek, Y., 2006, Timing and nature of postcollisional volcanism in western Anatolia and geodynamic implications, *in* Dilek, Y., and Pavlides, S., eds., Postcollisional tectonics and magmatism in the Mediterranean region and Asia: Geological Society of America Special Paper 409, p. 321–351, doi: 10.1130/2006.2409(17).

in the region. The asthenospheric melt contribution likely resulted from lithospheric delamination or partial convective removal of the subcontinental lithospheric mantle.

Alkaline volcanism, which started around 12 Ma and continued until the latest Quaternary, produced rocks in the tephrite, basanite, and foidite fields that show ocean island basalt–type trace-element patterns and $^{87}Sr/^{86}Sr$ (i) (0.7033 to 0.7030) and εNd (i) (+6.5 to +2.5) values. These features suggest enriched asthenospheric mantle–derived melts as their main magma source. Crustal contamination or assimilation was not an important process in the evolution of the alkaline group, suggesting that magma transport was facilitated by lithospheric-scale extensional fault systems that acted as natural conduits. Establishment of the Hellenic subduction zone and the associated slab roll-back from the middle Miocene onward produced arc volcanism on the south Aegean islands (Milos, Santorini, and Methana) and in southwestern Turkey (Bodrum). The postcollisional volcanism in western Anatolia thus displays compositionally distinct magmatic episodes controlled by slab break-off, lithospheric delamination, asthenospheric upwelling and decompressional melting, and oceanic lithospheric subduction as part of the geodynamic evolution of the eastern Mediterranean region throughout the Cenozoic.

Keywords: western Anatolia, Aegean extensional province, postcollisional volcanism, shoshonite, alkaline basalt, asthenospheric upwelling, slab break-off, lithospheric delamination

INTRODUCTION

The Neogene evolution of the eastern Mediterranean region was controlled mainly by three geodynamic processes: (1) continental collision of Arabia with Eurasia since the middle Miocene (ca. 13 Ma; McKenzie, 1978; Dewey et al., 1986; Jackson and McKenzie, 1988; Ring and Layer, 2003); (2) subduction of the Africa plate beneath Eurasia along the Hellenic and Cyprean trenches (LePichon and Angelier, 1979; Jackson and McKenzie, 1988; Kreemer et al., 2003); and (3) the westward escape of the Anatolian block away from the Arabia-Eurasia collision zone along the North and East Anatolian fault systems (Fig. 1; Ketin, 1948; McKenzie, 1972; Şengör and Yılmaz, 1981; Şengör et al., 1985; McKenzie and Yılmaz, 1991; Taymaz et al., 1991; Barka and Reilinger, 1997). Subduction roll-back processes along the Hellenic trench since 12–11 Ma (Meulenkamp et al., 1988) are believed to have caused extension in the upper plate, resulting in the development of the Aegean extensional province (Ring and Layer, 2003), which is presently undergoing ~north–south stretching as a whole in the range of 30–40 mm/yr (Taymaz et al., 1991; Oral, 1994; LePichon et al., 1995).

This north-south extension was accompanied by distinct pulses of volcanism throughout the late Neogene. However, the history of postcollisional magmatism in western Anatolia extends back to the Paleogene, as evidenced by the distribution of volcanic and plutonic rocks of this age throughout the region (Keller, 1983; Yılmaz, 1989, 1990; Güleç, 1991; Harris et al., 1994; Ercan et al., 1995; Richardson-Bunbury, 1996; Genç and Yılmaz, 1997; Savasçin and Oyman, 1998; Aldanmaz et al., 2000; Yılmaz et al., 2001). Postcollisional volcanism has occurred in distinct episodes throughout western Anatolia since the late Eocene and appears to have changed character from calc-alkaline to more alkaline and ultrapotassic over time (Yılmaz, 1989; Güleç, 1991; Seyitoğlu et al., 1997; Savasçin and Oyman, 1998; Aldanmaz et al., 2000; Altunkaynak et al., 2004). Because subduction of the African lithosphere beneath Eurasia along the Hellenic trench possibly dates back to the beginning of the Miocene at the earliest, the initial stages of calc-alkaline volcanism in western Anatolia during the late Eocene and the Oligocene were not related to any active subduction processes at that time. Therefore, the causes and magma sources of the early phases of postcollisional volcanism in this region remain significant questions for the geodynamic evolution of the Aegean extensional province (Pe-Piper and Piper, 2001, this volume).

Different models have been proposed to explain the tectonomagmatic evolution of Cenozoic volcanism in western Anatolia:

1. Collapse of the western Anatolian orogenic "welt" starting in the Oligo-Miocene, causing crustal attenuation and associated decompressional melting that produced the Paleogene–Neogene magmatism in the region (Seyitoğlu and Scott, 1992, 1996).
2. Subduction of the east Mediterranean ocean floor northward beneath Eurasia along the Hellenic trench and associated subduction zone magmatism (Fytikas et al., 1984; Pe-Piper and Piper, 1989; Gülen, 1990; Okay, 2002).

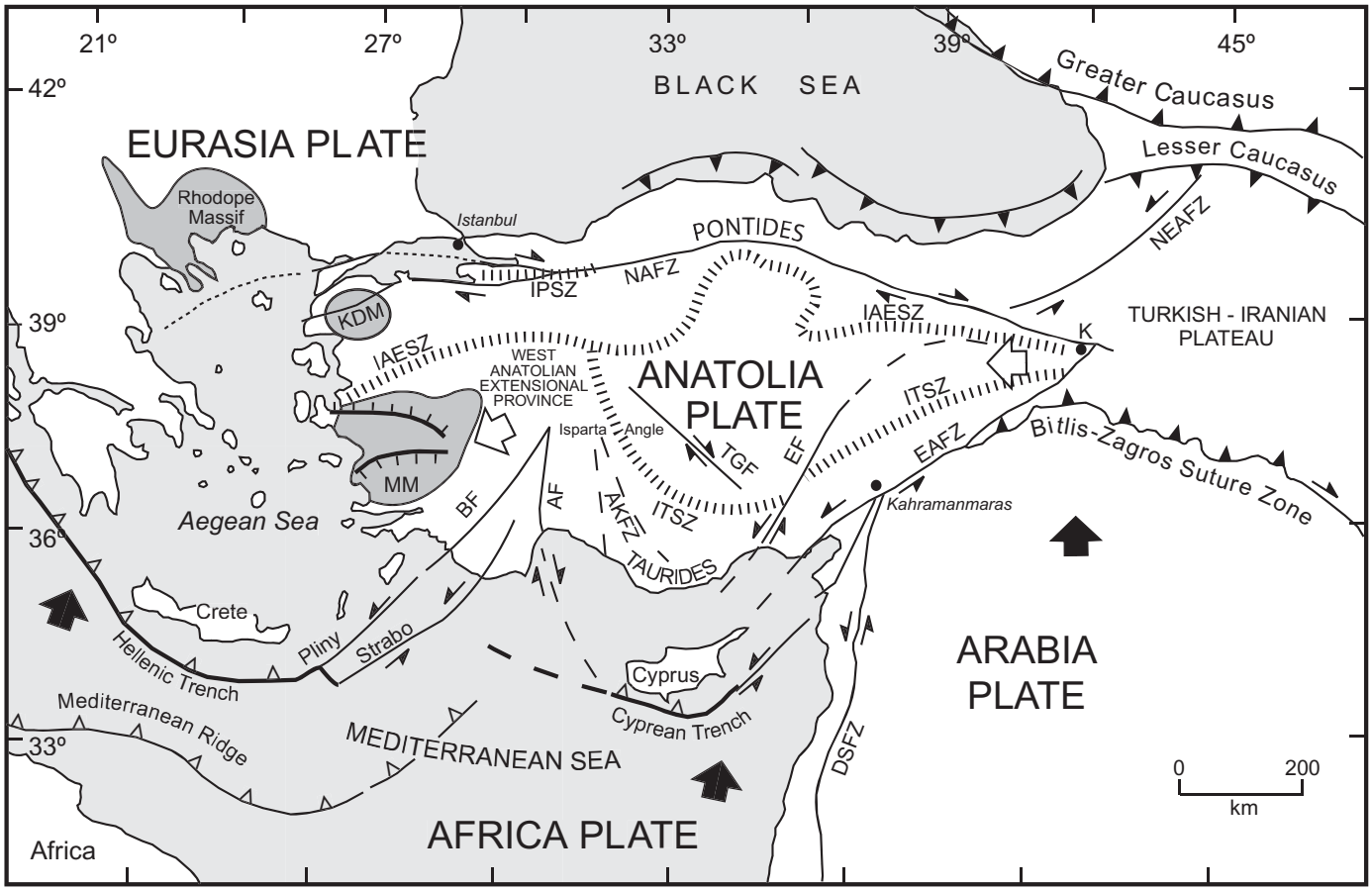

Figure 1. Simplified tectonic map of the eastern Mediterranean region showing major plate boundaries, plates, fault systems, and geological provinces relevant to this study (i.e., the West Anatolian extensional province, Rhodope massif, Taurides, Kazdag metamorphic massif [KDM], Menderes massif [MM], and Isparta angle). AF—Aksu fault; AKFZ—Akşehir fault zone; BF—Burdur fault; EAFZ—East Anatolian fault zone; EF—Ecemis fault; IAESZ—Izmir-Ankara-Erzincan suture zone; IPSZ—Intra-Pontide suture zone; ITSZ—Intra-Tauride suture zone; NAFZ—North Anatolian fault zone; NEAFZ—Northeast Anatolian fault zone; TGF—Tuz Gölü fault. The thick black arrows show the direction of plate convergence; the thick blank arrows depict the current motion of the Anatolia plate. Data are from Dewey et al. (1986); Yılmaz (1997); Bozkurt (2001); and Marchev et al. (2004).

3. Multiple episodes of magmatism in different tectonic regimes through time (Ercan et al., 1984, 1995; Yılmaz, 1989, 1990; Savaşçin and Güleç, 1990; Güleç, 1991), shifting from a north-south compression during the late Oligocene–early Miocene to north-south extension from the late Miocene onward (Ercan et al., 1984, 1995; Yılmaz, 1989, 1990; Altunkaynak and Yılmaz, 1998, 1999; Genç, 1998; Aldanmaz et al., 2000; Yılmaz et al., 2001).

Magmatism during the Eocene was limited mostly to northwestern Anatolia and produced mainly shallow-crustal granitic intrusions and their volcanic carapace (Yılmaz, 1992; Harris et al., 1994; Genç and Yılmaz, 1997; Genç, 1998). The Oligocene–early Miocene magmatism was characterized by intermediate to felsic plutonic, hypabyssal, and volcanic rocks that were closely related in space and time. The following magmatic phase during the late Miocene–Pliocene was marked by sporadic eruption of alkaline basaltic lavas (Borsi et al., 1972; Fytikas et al., 1984; Ercan et al., 1985; Yılmaz, 1989, 1990, 1997; Altunkaynak, 1996; Seyitoğlu et al., 1997; Altunkaynak and Yılmaz, 1998, 1999; Yılmaz et al., 2001).

The diversity of models and opinions on the causes and magma sources of Cenozoic volcanism in western Anatolia is in part a reflection of the complex geodynamic evolution of this region, but stems largely from the lack of systematic and comprehensive geochemical and geochronological data. Detailed field observations documenting the spatial and temporal relations between faulting and magmatism are also rare. Therefore, our

understanding of the possible links among magmatism, lithosphere kinematics, and mantle flow during the Cenozoic geodynamic evolution of western Anatolia is limited.

In this article, we review the existing geochemical and geochronological data from late Eocene and younger volcanic rocks in western Anatolia and present a systematic compositional classification of volcanic rock associations and their development through time. Based on the extant geochemical data and regional tectonic constraints, we evaluate the existing ideas and present an internally coherent geodynamic model for the postcollisional magmatic evolution of this region.

OVERVIEW OF THE GEOLOGY OF WESTERN ANATOLIA

The geology of western Anatolia consists of two distinct geological entities: basement units and cover sequences. Major components of the basement geology include the Sakarya continent, the Izmir-Ankara-Erzincan suture zone, metamorphic massifs (the Kazdag and Menderes massifs) and granitoid plutons, and the Tauride platform (Figs. 1 and 2). The cover sequences include latest Eocene and younger volcanic and sedimentary rocks that formed after the last episode of continental collision in the region during the early Eocene (Harris et al., 1994).

The Sakarya continent occurs between the Intra-Pontide suture to the north and the Izmir-Ankara-Erzincan suture zone to the south (Fig. 2) and consists of a Paleozoic crystalline basement with its Permo-Carboniferous sedimentary cover and Permo-Triassic ophiolitic and rift or accretionary-type mélange units (the Karakaya complex) collectively forming a composite continental block (Tekeli, 1981; Okay et al., 1996). The Tauride platform farther south is composed of carbonates and intercalated volcanosedimentary and epiclastic rocks ranging in age from Cambro-Ordovician to Lower Cretaceous (Ricou et al., 1975; Demirtasli et al., 1984; Özgül, 1984) and is tectonically overlain by Cretaceous ophiolite nappes derived from a Tethyan seaway to the north (Juteau, 1980; Dilek and Moores, 1990; Dilek et al., 1999a).

The Izmir-Ankara-Erzincan suture zone marks the site of the demise of a Neo-Tethyan seaway that had separated the Sakarya continent to the north from the Tauride platform to the south (Okay et al., 1998, and references therein; Tankut et al., 1998). A blueschist belt containing high-pressure metamorphic rocks of the northern passive margin of the Tauride platform occurs along the Izmir-Ankara-Erzincan suture zone and indicates that the subduction zone was dipping north beneath the Sakarya continent (Okay, 1984; Okay et al., 1998). The calculated *P-T* conditions of metamorphism and $^{40}Ar/^{39}Ar$ ages of phengites and glaucophanes from blueschist rocks suggest that metamorphism likely occurred over a period of ~20 m.y., from 108 Ma to 88 Ma (Harris et al., 1994). Southward emplacement of the Tethyan ophiolites and the blueschist metamorphism of the leading edge of the Tauride platform preceded a continent-continent collision between the Sakarya and Tauride continental blocks during the early Eocene (ca. 53–48 Ma; Harris et al., 1994). We consider this event the last alpine-style continental collision to have affected western Anatolia, and hence interpret all subsequent magmatism in the area as postcollisional in reference to this orogenic event. Much of western and central Anatolia was a highland marked by thickened continental crust (~55–60 km) and a high mean elevation (~3–4 km) in the aftermath of the Eocene collisional events in both western and central Anatolia (Şengör et al., 1985; Seyitoğlu and Scott, 1996; Dilek et al., 1999b; Dilek and Whitney, 2000).

The Kazdag and Menderes metamorphic massifs (Fig. 2) represent exhumed lower-crustal rocks in western Anatolia; hence, their evolutionary history points to the early stages of extensional tectonics in the region. Both massifs are analogous to Cordilleran-type core complexes and contain in their cores gneiss, amphibolite, and marble that were metamorphosed at >5 kbar and >600 °C. Rimmelé et al. (2003) estimated the *P-T* conditions of the metamorphic peak for the Menderes high-*P,* low-*T* rocks at >10 kbar and >440 °C. These massifs are overlain by relatively unmetamorphosed cover sequences and are intruded by synkinematic granitoids (Hetzel and Reischmann, 1996; Bozkurt and Park, 1997; Okay and Satir, 2000; Çemen et al., 2002; Gessner et al., 2004; Ring and Collins, 2005). The main episode of their metamorphism is inferred to have resulted from the burial regime that lasted from the Late Cretaceous to the latest Oligocene (Yılmaz, 2002). Estimated metamorphic pressures and the igneous age and *P-T* conditions of the crystallization of a granitoid pluton in the Kazdag massif suggest that its lower-crustal rocks were "rapidly exhumed at ~24 Ma from a depth of ~14 km to ~7 km" along a north-dipping mylonitic shear zone (Okay and Satir, 2002). Similarly, the Barrovian-type metamorphism of the Menderes massif occurred during the late Paleocene–early Eocene, as inferred from recent Rb-Sr mica ages (Bozkurt and Satir, 2000). Its unroofing took place in discrete extensional episodes dating back to the middle to late Eocene and continued through the early Miocene and the Pliocene, as constrained by recently obtained mica cooling ages (Bozkurt and Satir, 2000) and monazite ages (Catlos et al., 2002). Thus, the processes and timing of the initial postcollisional tectonic extension in western Anatolia are reasonably well constrained.

Figure 2. Simplified geological map of western Anatolia showing the distribution of volcanic rock groups (identified mainly based on their age relations), Cenozoic plutonic rocks mentioned in this article, and major metamorphic massifs. BG—Bakirçay graben; BMG—Büyük Menderes graben; CGD—Çataldag granodiorite; EP—Egrigöz pluton; GBG—Göynükbelen granite; GdG—Gediz graben; GG—Gördes graben; IAESZ—Izmir-Ankara-Erzincan suture zone; IGD—Ilica granodiorite; KG—Kozak granodiorite; KM—Kazdag massif; KMG—Küçük Menderes graben; OGD—Orhaneli granodiorite; SG—Selendi graben; TGD—Topuk granodiorite; UGB—Usak-Güre basin.

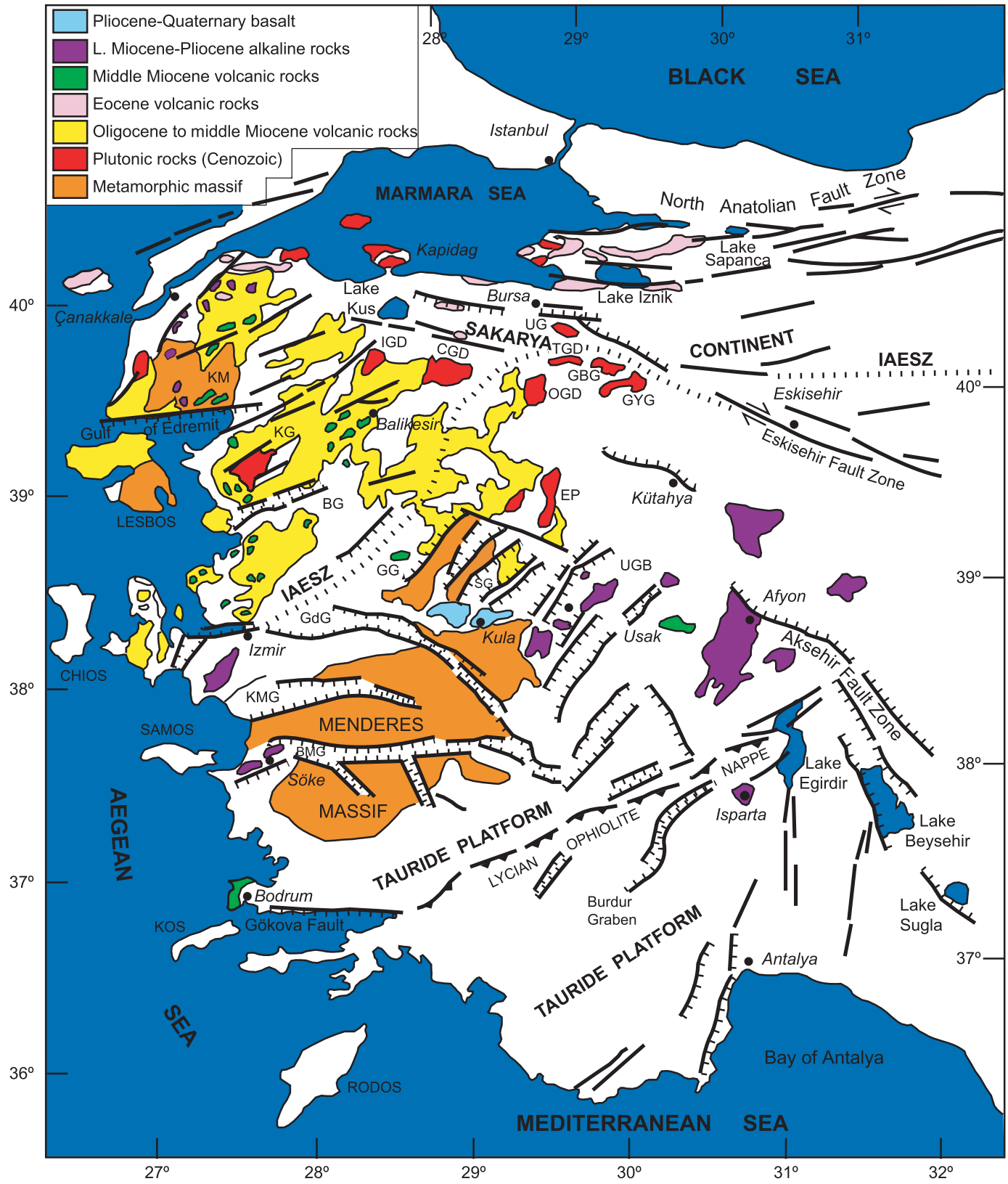
Pliocene-Quaternary basalt
L. Miocene-Pliocene alkaline rocks
Middle Miocene volcanic rocks
Eocene volcanic rocks
Oligocene to middle Miocene volcanic rocks
Plutonic rocks (Cenozoic)
Metamorphic massif
BLACK SEA
MARMARA SEA
Istanbul
Kapidag
Lake Kus
Bursa
Lake Iznik
North Anatolian Fault Zone
Lake Sapanca
Çanakkale
SAKARYA
UG
IGD
CGD
TGD
GBG
OGD
GYG
CONTINENT
IAESZ
Eskisehir
Eskisehir Fault Zone
KM
Gulf of Edremit
KG
Balikesir
BG
EP
Kütahya
LESBOS
GG
SG
UGB
IAESZ
GdG
Afyon
Kula
Usak
Izmir
Aksehir Fault Zone
CHIOS
KMG
MENDERES
SAMOS
BMG
Söke
MASSIF
NAPPE
Lake Egirdir
Isparta
Lake Beysehir
AEGEAN
TAURIDE PLATFORM
LYCIAN
OPHIOLITE
Burdur Graben
Bodrum
KOS
Gökova Fault
Lake Sugla
TAURIDE PLATFORM
Antalya
SEA
Bay of Antalya
RODOS
MEDITERRANEAN SEA
40°
39°
38°
37°
36°
28°
29°
30°
31°
27°
32°

Sedimentary rocks in the cover sequences start with upper Oligocene–lower Miocene lacustrine limestone, marl, and fine-grained clastic rocks that are widespread in western Anatolia. Upper Miocene coarse-grained clastic rocks represent the second phase of deposition in fault-bounded narrow basins and grabens (Yılmaz, 2002). There are two major sets of graben structures in western Anatolia (Fig. 2); earlier NNW- and NNE-trending grabens (i.e., the Gördes, Gediz, Selendi, and Usak-Güre grabens) are superimposed by younger east-west-trending larger (~5–15 km wide and 100–150 km long) grabens (i.e., the Edremit, Büyük Menderes, and Gökova grabens) that indicate strong north-south extension by the late Miocene (Yılmaz, 2002; Bozkurt, 2003).

Magmatic rocks in western Anatolia occur in three distinct associations: granitoid suites, intermediate to calc-alkaline volcanic sequences, and mafic volcanic units. Plutonic rocks comprise mainly granodiorites and monzonites with subordinate leucogranites and syenites, and the majority of these intrusions range in age from 30 to 16 Ma (Bingöl et al., 1982; Yılmaz, 1989, 1990; Altunkaynak and Yılmaz, 1998, 1999; Genç, 1998; Karacik and Yılmaz, 1998). Some older plutons (i.e., the Orhaneli and Topuk granodiorites, ca. 54–48 Ma) also occur and represent the very early phases of postcollisional magmatism in the region (Harris et al., 1994; Altunkaynak, 2004). These plutonic rocks are commonly accompanied by hypabyssal intrusions and locally intrude into their own extrusive carapace, indicating that they were emplaced at shallow crustal depths.

SUMMARY OF CENOZOIC VOLCANISM IN WESTERN ANATOLIA

The Cenozoic geology of western Anatolia is characterized by widespread volcanism that started in the late Eocene–early Oligocene and has continued up to the latest Quaternary (Savasçin and Dora, 1979; Fytikas et al., 1984; Bingöl et al., 1994; Harris et al., 1994; Savasçin and Erler, 1994). Extensive calc-alkaline volcanism occurred between 37 Ma and 16 Ma following the latest collisional event in the region that resulted in the development of significantly shortened and thickened continental crust. Eocene volcanic rocks and granitic plutons occur in an east-west-trending narrow zone along the southern edge of the Marmara Sea (in the northwestern part of the Biga Peninsula, on the Kapidag and Armutlu Peninsulas, and between Lakes Kus and Iznik, Fig. 2; Bingöl et al., 1994; Harris et al., 1994; Ercan et al., 1995; Genç and Yılmaz, 1997). Granitic plutons range in age from 53 Ma to 34.3 Ma and are intrusive into the basement rocks of the Sakarya continent. Principal exposures include the Topuk and Orhaneli (53–48 Ma), Armutlu (48.2–34.3 Ma), Lapseki (43.3 Ma), and Kapidag (42.2–36.1 Ma) plutons. These plutons are in general subalkaline in character and are composed of medium- to high-K monzogranite, granodiorite, and granite. Volcanic equivalents of these intrusive rocks consist of basaltic to andesitic lavas (the Kizderbent and Balikliçesme volcanics around Lake Iznik and the northwestern Biga Peninsula, respectively) and pyroclastic rocks. These subalkaline extrusive rocks range in composition from medium- to high-K series to shoshonites.

The next pulse of postcollisional volcanism is represented by intermediate to felsic volcanic rocks dated at 31–16 Ma, including andesite, trachyandesite, dacite, latite, and rhyolite, that are intercalated with pyroclastic and lacustrine deposits (Yılmaz, 1989; Bingöl et al., 1994; Altunkaynak and Yılmaz, 1998; Genç 1998; Karacik and Yılmaz, 1998; Savasçin and Oyman, 1998; Aldanmaz et al., 2000). These volcanic rocks are calc-alkaline in character and include plagioclase, hornblende, and/or orthopyroxene as their most common phenocrysts. This Oligo-Miocene volcanic activity was also spatially associated with mostly NNE- and partly northwest-trending transtensional fault systems (Altunkaynak, 1996; Altunkaynak and Yılmaz, 1998; Savasçin and Oyman, 1998; Yılmaz et al., 2000, 2001; Altunkaynak, 2004). Similar calc-alkaline and shoshonitic rocks dated 21.5–17 Ma also occur on the island of Lesbos to the west of the Gulf of Edremit (Fig. 2; Pe-Piper and Piper, 1992).

The major change from north-south compression to north-south extension in the region during the middle Miocene was accompanied by a gradual transition from calc-alkaline to alkaline basaltic volcanism (Aldanmaz et al., 2000; Yılmaz et al., 2001; Akay and Erdogan, 2004; Altunkaynak, 2004; Altunkaynak et al., 2004). Lavas of this stage are represented by mildly alkaline basalts (Yılmaz, 1989; Yılmaz et al., 2001; Altunkaynak et al., 2004) and are commonly seen to occur along NNE- and NNW-trending oblique transtensional fault systems (Altunkaynak and Yılmaz, 1998; Yılmaz et al., 2000; Altunkaynak, 2004). A transitional sequence consisting of andesitic rocks interspersed with and/or grading into dark, mildly alkaline basaltic lavas locally occurs between the calc-alkaline and mafic volcanic associations. The alkaline mafic volcanism in the region appears to have started in the late Miocene with shoshonitic to alkaline compositions and to have become more potassic and then sodic with time, as inferred from limited geochemical and geochronological data (Yılmaz, 1989; Savasçin and Oyman, 1998; Aldanmaz et al., 2000).

The final magmatic phase in western Anatolia is represented by rift-related volcanism characterized by strongly alkaline basaltic lavas of late Miocene to latest Quaternary age. Olivine-phyric and/or aphyric basalts and basanites with potassic-ultrapotassic compositions form the youngest episodes of volcanism (8.4 Ma to 0.13 ± 0.005 Ma; Richardson-Bunbury, 1996; Aldanmaz et al., 2000; Alıcı et al., 2002) and seem to be spatially associated with graben-bounding east-west-oriented normal fault systems and/or with the intersections of east-west- and northeast-trending grabens and fault systems.

GEOCHEMISTRY

Major- and Trace-Element Data

We identify three major groups of postcollisional volcanic rocks: a subalkaline group (SAG), a mildly alkaline group (MAG),

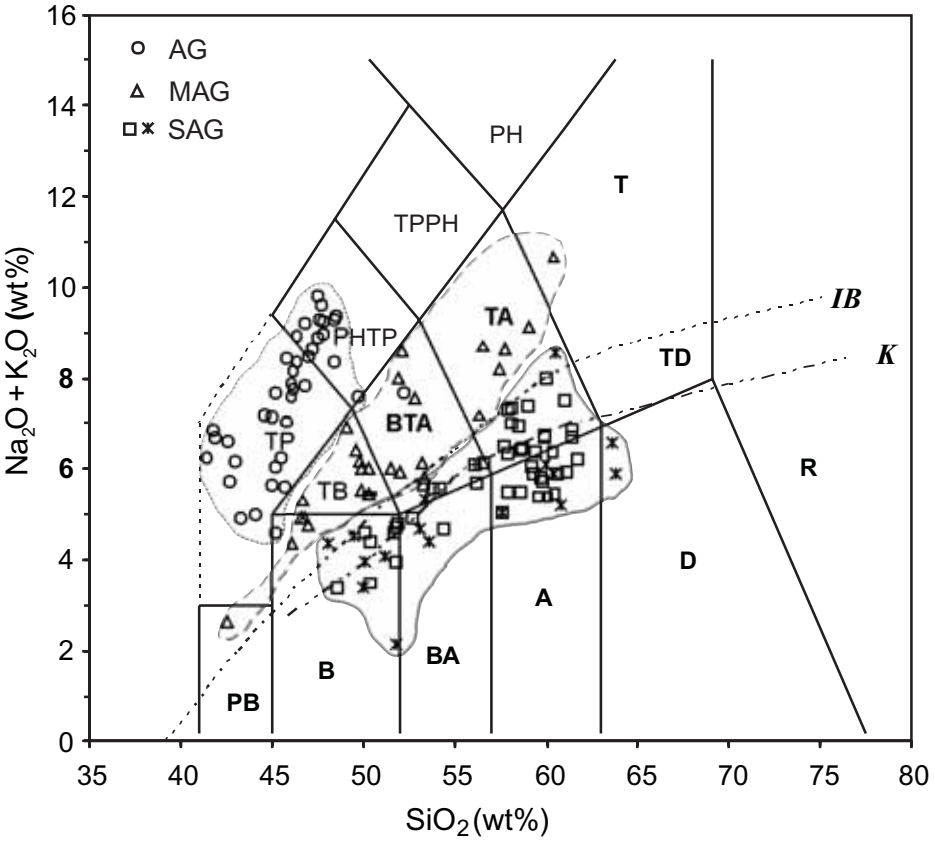

Figure 3. Total alkali versus SiO_2 classification diagram of the alkaline group (AG), mildly alkaline group (MAG), and subalkaline group (SAG), from Le Bas et al. (1986). A—andesite; B—basalt; BA—basaltic andesite; BS—basanite; BTA—basaltic trachy andesite; D—dacite; F—foidite; PC—picrobasalt; PH—phonolite; PHTP—phonotephrite; R—rhyolite; T—trachyte; TA—trachy andesite; TB—trachy basalt; TD—trachy dacite; TP—tephrite; TPPH—tephri phonolite. IB—alkali-subalkali subdivision, from Irvine and Baragar (1971), and K-alkali-subalkali subdivision from Kuno (1966).

and an alkaline group (AG) (Fig. 3; Tables 1, 2, 3, and 4), based on their major- and trace-element compositions.

Subalkaline Group. Rocks of the SAG are further subdivided into two groups based on their known ages: an Eocene subalkaline group (ESAG) and an Oligocene–early Miocene subalkaline group (OMSAG). The ESAG consists mainly of basalt, basaltic andesite, andesite, trachy-andesite, and dacite. The TiO_2 contents of these rocks range from 0.58 to 2.13 wt%, and their Al_2O_3 abundances are medium to high (15–18 wt%). The majority of ESAG lavas classify mainly as medium- to high-K calc-alkaline in a K_2O versus Na_2O diagram, although some of them belong to shoshonitic series (Fig. 4). In general, ESAG rocks have low to moderate MgO contents (0.70–6.23 wt%) (Fig. 5). In the MgO variation diagrams, their SiO_2 and Al_2O_3 values increase, whereas their CaO and Fe_2O_3 values decrease with decreasing MgO. These rocks have the lowest trace-element contents compared to other groups (OMSAG, MAG, and AG) but show similar trends of trace-element distribution patterns (e.g., Ni, Sr, Rb, and La) against MgO. The Rb and La values decrease with increasing MgO, and the Sr concentrations (176–434 ppm) are relatively constant over a range of MgO (wt%) from 6 to 1; however, the combined array that includes all groups (ESAG, OMSAG, MAG, and AG) shows a decrease in Sr content with decreasing MgO (Fig. 5).

In a mid-ocean ridge basalt (MORB)–normalized trace-element variation diagram (Fig. 6), the ESAG rocks display enrichment in large-ion lithophile elements (LILE) (K, Rb, Ba, Th, Sr) over light rare earth elements (LREE) and middle rare earth elements (MREE), as reflected by the Ba/La (6–19.57), K/La (104–1235), Th/La (0.17–1), and Rb/La (0.25–4.05) ratios, and depletion in high field strength elements (HFSE) (Zr, Nb, Ti, and P) with respect to neighboring LILE and fractionation among LILE (Rb, Ba, and K). Trace-element variations and interelement ratios collectively suggest that magmas of the ESAG show similar patterns to those of subduction-related arc magmas (Fig. 6; Pearce, 1982; Thorpe et al., 1982; Cox and Hawkesworth, 1985; Pearce et al., 1990; Davidson et al., 1991; Saunders et al., 1991; Walker et al., 1991; Hawkesworth et al., 1993; Pearce and Peate, 1995). However, their trace-element abundances, such as Ba (50–313 ppm), Th (2–13 ppm), and La (2–25 ppm), show that the ESAG lavas were moderately enriched in incompatible elements, indicating that their melts were moderately evolved (Frey et al., 1978; Gill, 1981; Pearce, 1982).

The OMSAG is seen to be composed mainly of dacite, andesite, basaltic andesite, and basalt in the total alkalis versus silica diagram (Le Bas et al., 1986; Fig. 3), with a silica content ranging from 48 to 63 wt%. These subalkaline lavas are TiO_2-depleted (<1 wt%), with medium to high Al_2O_3 abundances

TABLE 1. REPRESENTATIVE CHEMICAL ANALYSES OF THE EOCENE SUBALKALINE GROUP FROM WESTERN ANATOLIA

Sample no.	GG20b	GG21b	GG65	GG175	SZ26	CG51	CG66	KY19	KY21	KY23	KY63	KY29	KY32	KY33	KY50	55
Source of data	1	1	1	1	1	1	1	2	2	2	2	2	2	2	2	3
SiO_2	57.56	53.54	59.97	51.78	60.54	49.92	63.75	50.07	51.26	48.11	49.45	60.85	53.35	60.39	53.06	63.59
TiO_2	0.71	0.66	0.73	1.03	0.65	1.25	0.66	1.60	1.30	1.70	2.13	0.79	1.19	0.69	1.07	0.58
Al_2O_3	15.61	15.88	15.74	16.63	15.49	16.85	15.97	16.49	18.42	17.37	16.43	16.22	18.4	17.82	16.83	16.44
Fe_2O_3	6.59	6.44	5.45	8.63	4.80	10.61	4.85	11.42	10.82	10.93	13.12	6.18	9.05	5.75	8.56	5.13
MnO	0.11	0.13	0.14	0.18	0.11	0.18	0.11	0.19	0.18	0.18	0.16	0.11	0.20	12.00	0.07	0.14
MgO	5.87	4.64	2.32	5.67	2.89	6.27	1.43	5.73	4.92	3.46	4.35	0.70	3.00	1.45	5.78	1.47
CaO	6.23	7.03	5.37	11.92	1.81	10.15	4.59	9.27	8.65	9.03	7.79	6.54	7.87	5.61	6.67	4.41
Na_2O	3.61	2.80	3.45	2.05	4.95	2.81	3.37	3.25	3.59	3.74	3.43	3.92	4.48	4.14	4.40	3.40
K_2O	1.41	1.61	2.64	0.10	3.57	0.59	2.53	0.72	0.49	0.64	1.08	1.25	0.86	1.74	0.28	3.15
P_2O_5	0.23	0.18	0.27	0.16	0.23	0.08	0.19	0.29	0.19	0.48	0.39	0.32	0.24	0.29	0.20	0.16
LOI	2.02	5.34	2.62	4.63	3.73	3.3	2.33	0.84	0.89	0.86	0.99	3.90	2.92	2.93	5.61	0.87
Total	99.90	98.25	98.70	102.70	98.77	102.01	99.78	99.97	99.71	96.5	99.32	100.80	101.60	100.90	102.50	99.34
Sr	317	305	211	290	104	262	219	281	272	315	219	176	270	284	200	434
Ba	313	267	224	50	180	137	223	144	131	163	180	26	225	208	57	743
Rb	42	47	73	2	76	14	68	10	8	8	30	30	21	41	6	70
Ni	32	31	11	n.d	11	16	n.d	43	33	12	22	1	7	1	14	<20
Co	16	15	9	26	6	34	9	61	108	61	51	14	33	31	39	n.d.
Cr	62	57	15	n.d	11	n.d	6	94	16	7	10	1	12	3	16	<20
V	140	144	69	202	53	379	67	285	252	252	297	31	182	53	191	200
Zr	181	175	216	112	239	78	212	167	115	224	231	292	152	227	131	155
Y	20	20	34	20	31	25	37	35	27	39	49	56	34	39	26	24
Nb	8	7	12	7	11	4	12	1	1	3	2	5	2	4	6	11
La	17	17	18	8	20	7	17	24	18	12	22	25	2	28	n.d	27.6
Ce	42	44	52	26	41	15	38	24	21	53	45	46	31	29	29	52
Pr	n.d.	n.d.	n.d.	n.d.	n.d.	n.d.	n.d.	n.d.	n.d.	n.d.	n.d.	n.d.	n.d.	n.d.	n.d.	6
Nd	20	20	26	n.d.	n.d.	n.d.	n.d.	n.d.	n.d.	n.d.	n.d.	n.d.	n.d.	n.d.	n.d.	22.4
Sm	n.d.	n.d.	14	27	9	23	n.d.	n.d.	n.d.	n.d.	n.d.	n.d.	n.d.	n.d.	n.d.	4.4
Eu	n.d.	n.d.	n.d.	n.d.	n.d.	n.d.	n.d.	n.d.	n.d.	n.d.	n.d.	n.d.	n.d.	n.d.	n.d.	1.2
Gd	n.d.	n.d.	n.d.	n.d.	n.d.	n.d.	n.d.	n.d.	n.d.	n.d.	n.d.	n.d.	n.d.	n.d.	n.d.	8.1
Tb	n.d.	n.d.	n.d.	n.d.	n.d.	n.d.	n.d.	n.d.	n.d.	n.d.	n.d.	n.d.	n.d.	n.d.	n.d.	0.59
Dy	n.d.	n.d.	n.d.	n.d.	n.d.	n.d.	n.d.	n.d.	n.d.	n.d.	n.d.	n.d.	n.d.	n.d.	n.d.	3.83
Er	n.d.	n.d.	n.d.	n.d.	n.d.	n.d.	n.d.	n.d.	n.d.	n.d.	n.d.	n.d.	n.d.	n.d.	n.d.	2.32
Tm	n.d.	n.d.	n.d.	n.d.	n.d.	n.d.	n.d.	n.d.	n.d.	n.d.	n.d.	n.d.	n.d.	n.d.	n.d.	0.34
Yb	n.d.	n.d.	n.d.	n.d.	n.d.	n.d.	n.d.	n.d.	n.d.	n.d.	n.d.	n.d.	n.d.	n.d.	n.d.	2.37
Lu	n.d.	n.d.	n.d.	n.d.	n.d.	n.d.	n.d.	n.d.	n.d.	n.d.	n.d.	n.d.	n.d.	n.d.	n.d.	0.37
Hf	n.d.	n.d.	n.d.	n.d.	n.d.	n.d.	n.d.	n.d.	n.d.	n.d.	n.d.	n.d.	n.d.	n.d.	n.d.	2
Cs	n.d.	n.d.	n.d.	n.d.	n.d.	n.d.	n.d.	n.d.	n.d.	n.d.	n.d.	n.d.	n.d.	n.d.	n.d.	0.46
Pb	14	17	12	n.d	15	10	12	5	3	4	7	17	1	1	6	10
Ta	n.d.	n.d.	n.d.	n.d.	n.d.	n.d.	n.d.	n.d.	n.d.	n.d.	n.d.	n.d.	n.d.	n.d.	n.d.	0.7
Th	9	11	13	7	12	7	11	5	6	6	6	12	7	5	2	9.04
U	n.d.	n.d.	n.d.	n.d.	n.d.	n.d.	n.d.	n.d.	n.d.	n.d.	n.d.	n.d.	n.d.	n.d.	n.d.	1.62
$^{87}Sr/^{86}Sr$	n.d.	n.d.	n.d.	n.d.	n.d.	n.d.	n.d.	n.d.	n.d.	n.d.	n.d.	n.d.	n.d.	n.d.	n.d.	0.7059
$^{143}Nd/^{144}Nd$	n.d.	n.d.	n.d.	n.d.	n.d.	n.d.	n.d.	n.d.	n.d.	n.d.	n.d.	n.d.	n.d.	n.d.	n.d.	0.5125

Sources: Data taken from (1) Genç and Yılmaz (1997); (2) Yılmaz (1992); (3) Ercan et al. (1995).
Note: n.d—not determined.

TABLE 2. REPRESENTATIVE CHEMICAL ANALYSES OF THE OLIGOCENE–EARLY MIOCENE SUBALKALINE GROUP FROM WESTERN ANATOLIA

Sample no.	EA380	EA143	16	EA348	EA407	35	37	39	17	18	19B	20B	21B	EA278	EA53	EA45	EA55	EA418	EA67
Source of data	1	1	1	1	1	This study	This study	This study	This study	This study	This study	This study	This study	1	1	1	1	1	1
SiO_2	50.35	52.69	51.88	54.40	56.64	51.79	48.60	50.11	53.34	53.81	50.32	51.76	51.85	59.40	58.95	57.73	58.09	56.24	59.96
TiO_2	0.93	0.85	0.82	0.73	1.03	0.84	1.00	0.93	1.1	1.19	1.01	0.99	0.99	0.70	0.83	0.73	0.83	0.87	0.75
Al_2O_3	15.37	15.68	16.20	15.36	17.16	18.98	16.00	17.77	17.14	16.60	14.26	17.85	17.88	17.10	19.75	16.71	19.25	18.45	16.38
Fe_2O_3	8.27	7.44	6.89	7.36	7.43	8.94	10.80	8.88	7.43	7.74	8.75	7.64	7.99	6.90	4.74	5.74	5.05	6.40	5.89
MnO	0.14	0.13	0.11	0.12	0.08	0.19	0.20	0.17	0.13	0.12	0.15	0.14	0.14	0.15	0.07	0.09	0.08	0.09	0.06
MgO	9.81	7.53	6.79	9.06	2.04	4.66	7.90	2.99	4.61	4.58	9.93	3.52	4.29	2.87	1.15	3.75	1.19	3.83	2.33
CaO	9.55	10.01	8.73	8.25	8.83	9.65	10.2	9.44	7.79	7.57	11.03	9.08	8.65	6.33	6.31	6.78	6.96	7.9	5.42
Na_2O	2.22	2.58	2.83	2.78	3.37	3.06	2.30	2.94	3.4	3.38	2.51	3.05	3.14	3.11	3.98	3.43	4.04	3.87	3.22
K_2O	2.18	2.33	1.95	1.89	2.76	0.92	1.10	1.64	2.25	2.21	1.00	1.56	1.56	3.27	3.42	3.07	3.31	1.84	4.77
P_2O_5	0.32	1.82	0.26	0.24	0.32	0.17	0.20	0.29	0.48	0.35	0.24	0.26	0.27	0.22	0.35	0.25	0.33	0.29	0.40
LOI	1.82	1.82	96.46	1.27	1.14	0.33	1.20	3.98	2.00	2.20	0.50	3.90	3.00	1.43	1.49	1.58	2.64	1.26	1.43
Total	99.14	99.50	193.02	100.19	99.66	99.53	99.50	99.14	99.85	99.9	99.89	99.85	99.87	100.05	99.55	98.28	99.13	99.78	99.19
Sr	1006.5	627.8	537.0	714.6	637.8	510.0	510.0	509.0	717.9	568.8	785.7	848.7	808.9	574.0	1037.2	826.6	1018.2	944.8	960.4
Ba	1436.7	1095.7	675.0	1164.0	919.8	267.0	200.0	678.0	1344.0	1173.0	841.0	900.0	900.0	123.0	1595.5	1309.4	1553.5	1358.2	1515.0
Rb	63.1	81.5	96.0	63.3	98.6	26.0	22.0	36.0	64.5	60.3	24.6	69.6	65.8	844.0	122.9	107.5	119.3	68.3	189.7
Ni	163.9	167.1	135.0	222.3	44.5	20.0	20.0	21.0	55.0	22.0	107.0	20.0	23.0	4.3	18.6	37.7	12.3	37.7	21.9
Co	34.8	34.4	30.0	34.4	15.6	n.d.	n.d.	n.d.	21.7	26.3	42.2	26.5	27.3	n.d.	6.1	17.8	10.5	24.7	n.d.
Cr	400.5	338.2	366.0	464.3	166.3	20.0	40.0	33.0	n.d.	n.d.	n.d.	n.d.	n.d.	n.d.	4.5	76.8	13.6	38.6	48.0
V	225.7	167.1	174.0	161.6	154.9	100.0	300.0	224.0	144.0	165.0	204.0	182.0	172.0	131.3	139.1	146.7	169.2	190.9	n.d.
Zr	119.4	139.8	154.30	127.3	191.5	72	140	131	227.1	211.5	98.8	134.6	134.9	196	248	204	240.6	184.7	248.4
Y	22	23.6	22.7	21.5	23.8	22	19	29	30.5	29.5	21.5	26.8	24.8	28.8	20.9	21.5	21.1	22	29.6
Nb	11.1	9.4	14.30	7.5	17.3	4	23	6	17.8	14.9	7.5	8.5	8.2	11.7	11.9	10.3	11.1	8.5	15.9
Ga	14.6	16.7	n.d.	13.1	18.7	n.d.	n.d.	n.d.	18.7	20.5	14.2	19.4	19.0	17.0	20.0	18.0	21.0	20.0	20.0
La	42.28	34.75	38.30	31.92	46.44	n.d.	n.d.	n.d.	51.70	36.80	20.70	35.50	35.30	39.69	66.85	60.14	68.36	52.15	92.79
Ce	81.30	68.03	72.20	62.67	84.08	n.d.	n.d.	n.d.	89.40	64.50	37.70	63.80	61.80	79.08	127.17	113.74	127.43	100.19	178.90
Pr	9.32	7.55	8.33	7.09	9.11	n.d.	n.d.	n.d.	10.08	7.29	4.28	7.23	6.9	8.89	13.84	12.26	13.83	11.14	20.00
Nd	37.73	30.63	30.33	28.84	35.31	n.d.	n.d.	n.d.	41.20	31.20	20.60	32.80	31.00	35.29	52.80	46.85	52.75	43.49	77.73
Sm	6.49	5.79	5.49	5.31	5.76	n.d.	n.d.	n.d.	7.70	5.40	4.10	6.60	6.00	6.44	7.89	7.36	7.90	7.06	12.93
Eu	1.76	1.45	1.41	1.39	1.54	n.d.	n.d.	n.d.	1.85	1.58	1.25	1.44	1.44	1.50	1.94	1.69	1.88	1.77	2.76
Gd	4.98	4.86	4.62	4.44	4.56	n.d.	n.d.	n.d.	6.45	5.38	4.29	4.81	4.80	5.30	5.24	5.00	5.22	5.11	8.84
Tb	0.74	0.71	0.69	0.67	0.70	n.d.	n.d.	n.d.	0.93	0.83	0.68	0.73	0.74	0.84	0.72	0.72	0.72	0.73	1.17
Dy	3.96	3.87	3.90	3.69	3.90	n.d.	n.d.	n.d.	4.88	4.51	3.29	4.38	4.12	4.68	3.69	3.77	3.66	3.86	5.48
Er	1.91	2.10	2.19	1.98	2.17	n.d.	n.d.	n.d.	2.86	2.69	2.17	2.37	2.39	2.64	1.79	1.94	1.80	1.95	2.33
Tm	0.32	0.35	0.35	0.39	n.d.	n.d.	n.d.	0.50	0.42	0.27	0.37	0.28	0.47	0.30	0.34	0.31	0.33	0.38	n.d.
Yb	1.76	2.11	2.11	1.97	2.26	n.d.	n.d.	n.d.	2.88	2.83	1.75	2.34	2.47	2.78	1.78	1.96	1.77	1.91	2.12
Lu	0.28	0.33	0.324	0.31	0.36	n.d.	n.d.	n.d.	0.48	0.43	0.30	0.39	0.44	0.45	0.27	0.31	0.27	0.30	0.33
Hf	3.02	3.48	4.06	3.22	4.73	n.d.	n.d.	n.d.	5.40	5.70	2.1	3.4	3.20	4.61	6.22	5.41	6.00	4.75	5.89
Cs	4	5.30	1.80	4.70	n.d.	n.d.	n.d.	2.6	6.60	8.10	7.50	8.60	6.60	3.70	3.77	7.00	6.40	6.30	n.d.
Pb	n.d.	18.50	17.43	n.d.	n.d.	n.d.	n.d.	n.d.	n.d.	12.20	n.d.	n.d.	6.10	n.d.	n.d.	n.d.	n.d.	n.d.	n.d.
Ta	0.65	0.64	0.89	0.53	1.29	n.d.	n.d.	n.d.	1.1	1.10	0.50	0.60	0.60	0.89	0.76	0.72	0.73	0.56	1.39
Th	14.71	14.02	14.69	12.16	18.57	n.d.	n.d.	n.d.	13.6	12.90	6.30	12.6	12.40	20.55	29.32	26.22	28.2	17.95	52.12
U	2.73	2.98	3.20	2.69	5.35	n.d.	n.d.	n.d.	2.30	2.40	1.50	4.10	3.10	6.18	5.49	5.17	5.42	3.48	13.46
$^{87}Sr/^{86}Sr$	n.d.	n.d.	0.7076	0.7081	n.d.	0.7048	n.d.	n.d.	n.d.	n.d.	n.d.	n.d.	0.7067	n.d.	n.d.	n.d.	n.d.	0.7084	n.d.
$^{143}Nd/^{144}Nd$	n.d.	0.5123	0.5124	n.d.	n.d.	n.d.	n.d.	n.d.	n.d.	n.d.	n.d.	0.5129	n.d.	n.d.	n.d.	n.d.	n.d.	0.5120	n.d.

(continued)

TABLE 2. *Continued*

Sample no.	EA113	EA346	EA314	EA334	EA155	SE12	11698	28166	TM81-981	TM81-904	TM81-316	16	17	18	19	20	21
Source of data	1	1	1	1	1	2	3	3	3	3	3	4	4	4	4	4	4
SiO_2	60.62	60.41	60.32	59.64	59.80	59.75	61.37	61.44	59.12	59.28	61.68	58.10	58.60	59.60	57.90	61.12	59.89
TiO_2	0.72	0.64	0.59	0.57	0.73	0.82	0.74	0.61	0.74	0.74	0.69	0.80	1.00	1.00	0.88	0.64	0.60
Al_2O_3	16.41	15.88	17.17	15.95	16.32	16.97	15.68	16.73	16.26	17.24	17.25	16.60	16.50	16.80	16.38	15.69	15.94
Fe_2O_3	6.76	5.80	5.35	5.95	7.08	6.36	6.16	5.58	6.30	6.91	6.21	6.40	7.80	7.90	7.36	6.12	5.58
MnO	0.12	0.10	0.10	0.12	0.16	0.11	0.07	0.05	0.12	0.11	0.04	0.10	0.30	0.10	0.15	0.05	0.10
MgO	2.53	4.29	4.66	5.08	2.57	3.68	2.27	2.57	3.43	2.42	1.05	2.90	2.50	1.60	2.36	2.14	2.19
CaO	6.62	6.29	5.87	7.30	5.66	6.74	5.12	5.07	6.49	5.88	5.60	5.30	6.60	4.90	6.64	6.01	6.01
Na_2O	3.42	2.88	3.69	3.30	3.14	3.10	2.96	3.51	3.26	3.41	3.63	3.00	3.20	2.60	3.38	3.42	3.73
K_2O	2.47	2.57	2.67	2.51	3.54	2.64	3.88	3.17	2.78	2.47	2.59	4.00	3.20	2.80	2.95	2.52	2.99
P_2O_5	0.21	0.16	0.14	0.15	0.25	0.23	0.39	0.20	0.19	0.12	0.19	0.30	0.30	0.20	0.25	0.27	0.28
LOI	0.88	1.33	0.99	1.70	2.82	1.49	1.12	0.72	1.32	1.30	0.99	1.40	0.60	2.20	1.09	1.39	2.08
Total	99.88	99.02	100.60	100.56	99.224	100.43	99.76	99.65	99.99	99.87	99.93	98.90	100.60	99.70	99.34	99.37	99.39
Sr	675.90	576.5	441.1	611.8	773.3	674	640	492	507	466	411	784	816	846	737	1071	1004
Ba	1193.0	1195.0	748.0	1045.6	1483.1	1206.0	1347.0	1151.0	966.0	775.0	861.0	1000.0	700.0	2000.0	964.0	975.0	1171.0
Rb	74.40	83.60	108.40	113.00	125.40	101.00	140.00	115.00	106.00	71.00	93.00	114.00	95.00	87.00	92.00	77.00	0.88
Ni	9.4	35.7	83.6	39.5	17.7	9.0	24.0	23.0	14.0	3.0	10.0	20.0	20.0	20.0	19.0	76.0	14.0
Co	n.d.	n.d.	n.d.	n.d.	n.d.	n.d.	n.d.	n.d.	n.d.	n.d.	n.d.	n.d.	n.d.	n.d.	n.d.	n.d.	n.d.
Cr	17.8	128.7	204.6	36	60.3	240.0	87.0	44.0	51.0	5.0	19.0	<20.0	<20.0	<20.0	37.0	346.0	30.0
V	161	123	103	191	150.4	200.0	98.0	85.0	139.0	149.0	128.0	100.0	150.0	200.0	218.0	153.0	148.0
Zr	143	141	148	115	156	180	201	173	176	136	188	297	291	270	177	148	176
Y	28.7	22.5	21.3	22.4	21.0	29.0	31.0	24.0	26.0	34.0	34.0	31.0	38.0	30.0	31.0	18.0	19.0
Nb	6.7	8.1	9.7	7.7	8.8	10.9	13.0	13.0	12.0	9.0	9.0	23.0	13.0	12.0	1.0	0.3	2.0
Ga	19.0	17.0	15.0	19.0	16.8	19.0	n.d.	n.d.	n.d.	n.d.	n.d.	n.d.	n.d.	n.d.	n.d.	n.d.	n.d.
La	37.54	31.02	29.33	34.05	44.69	205.00	n.d.	n.d.	n.d.	n.d.	n.d.	n.d.	n.d.	n.d.	36.70	n.d.	n.d.
Ce	74.01	59.47	57.14	64.62	88.25	446.00	n.d.	n.d.	n.d.	n.d.	n.d.	n.d.	n.d.	n.d.	70.00	n.d.	n.d.
Pr	8.05	6.43	6.28	6.90	9.61		n.d.	n.d.	n.d.	n.d.	n.d.	n.d.	n.d.	n.d.	8.70	n.d.	n.d.
Nd	31.36	25.3	24.31	27.02	35.65	192.00	36.73	31.18	26.50	26.30	44.67	n.d.	n.d.	n.d.	34.40	n.d.	n.d.
Sm	5.98	4.75	4.45	4.96	6.14		7.00	5.50	5.00	5.80	8.50	n.d.	n.d.	n.d.	7.00	n.d.	n.d.
Eu	1.67	1.22	1.08	1.15	1.45	n.d.	n.d.	n.d.	n.d.	n.d.	n.d.	n.d.	n.d.	n.d.	1.78	n.d.	n.d.
Gd	5.33	4.15	3.7	4.27	4.59	n.d.	n.d.	n.d.	n.d.	n.d.	n.d.	n.d.	n.d.	n.d.	6.02	n.d.	n.d.
Tb	0.81	0.65	0.62	0.65	0.66	n.d.	n.d.	n.d.	n.d.	n.d.	n.d.	n.d.	n.d.	n.d.	0.86	n.d.	n.d.
Dy	4.59	3.65	3.53	3.63	3.53	n.d.	n.d.	n.d.	n.d.	n.d.	n.d.	n.d.	n.d.	n.d.	5.36	n.d.	n.d.
Er	2.53	20.1	1.96	2.00	1.76	n.d.	n.d.	n.d.	n.d.	n.d.	n.d.	n.d.	n.d.	n.d.	3.35	n.d.	n.d.
Tm	0.44	0.34	0.35	0.34	0.30	n.d.	n.d.	n.d.	n.d.	n.d.	n.d.	n.d.	n.d.	n.d.	0.47	n.d.	n.d.
Yb	2.63	2.08	2.05	2.06	1.77	n.d.	n.d.	n.d.	n.d.	n.d.	n.d.	n.d.	n.d.	n.d.	3.05	n.d.	n.d.
Lu	0.42	0.32	0.33	0.32	0.28	n.d.	n.d.	n.d.	n.d.	n.d.	n.d.	n.d.	n.d.	n.d.	0.42	n.d.	n.d.
Hf	2.93	3.64	4.00	2.90	2.57	n.d.	n.d.	n.d.	n.d.	n.d.	n.d.	n.d.	n.d.	n.d.	3.91	n.d.	n.d.
Cs	6.30	2.80	4.50	1.70	4.40	n.d.	n.d.	n.d.	n.d.	n.d.	n.d.	n.d.	n.d.	n.d.	2.51	n.d.	n.d.
Pb	21.50	20.40	n.d.	n.d.	n.d.	n.d.	21.00	20.00	n.d.	n.d.	n.d.	n.d.	n.d.	21.57	n.d.	n.d.	n.d.
Ta	0.57	0.59	0.89	0.69	0.78	n.d.	n.d.	n.d.	n.d.	n.d.	n.d.	n.d.	n.d.	n.d.	0.48	n.d.	n.d.
Th	16.00	11.48	14.47	14.64	21.92	20.00	n.d.	n.d.	n.d.	n.d.	n.d.	n.d.	n.d.	n.d.	16.28	n.d.	n.d.
U	5.05	2.82	4.20	3.72	4.76	n.d.	n.d.	n.d.	n.d.	n.d.	n.d.	n.d.	n.d.	n.d.	4.86	n.d.	n.d.
$^{87}Sr/^{86}Sr$	n.d.	n.d.	0.7090	n.d.	n.d.	n.d.	0.7090	0.7088	0.7070	0.7086	0.7086	n.d.	n.d.	n.d.	n.d.	n.d.	n.d.
$^{143}Nd/^{144}Nd$	n.d.	n.d.	0.51200	n.d.	n.d.	n.d.	0.51200	0.51200	0.51240	0.51240	0.51242	n.d.	n.d.	n.d.	n.d.	n.d.	n.d.

Sources: Data taken from (1) Aldanmaz et al. (2000); (2) Seyitoğlu et al. (1997); (3) Güleç (1991); (4) Ercan et al. (1995).
Note: n.d.—not determined.

TABLE 3. REPRESENTATIVE CHEMICAL ANALYSES OF THE MILDLY ALKALINE GROUP FROM WESTERN ANATOLIA

Sample no.	UG8	UG7	10	EA399	30	40	13	43	44	45	EA385	UG145	E3	12	TM-9-53	3	UG142	EA413
Source of data	1	1	2	3	This study	This study	This study	This study	This study	This study	3	1	1	4	5	4	1	3
SiO_2	53.28	53.22	42.65	49.82	50.10	47.62	53.13	48.09	45.98	47.05	50.26	57.67	57.42	58.92	51.93	46.80	60.30	56.29
TiO_2	1.21	1.20	0.57	1.19	0.96	1.35	1.30	1.18	1.38	1.30	1.05	2.07	1.91	0.46	1.77	2.90	2.02	1.07
$A_{l2}O_3$	16.41	16.36	11.07	17.30	16.55	17.80	17.04	16.60	16.68	16.60	19.23	12.99	14.25	16.41	11.61	14.00	14.47	19.30
Fe_2O_3	8.02	8.03	7.28	8.50	7.47	9.14	8.29	8.33	9.12	9.35	8.09	6.77	7.05	3.97	6.84	13.00	6.07	6.20
MnO	0.13	0.13	0.13	0.16	0.16	0.16	0.16	0.15	0.15	0.17	0.15	0.06	0.09	0.08	0.11	0.20	0.08	0.08
MgO	7.45	7.25	10.12	5.94	6.12	7.73	2.94	8.00	7.26	5.89	4.83	5.42	4.89	1.03	7.72	7.30	2.66	2.06
CaO	7.92	7.75	11.11	9.67	8.72	11.91	6.39	10.48	12.11	11.12	9.52	5.73	6.78	4.27	8.24	9.70	3.66	6.53
Na_2O	2.63	2.91	1.47	4.33	4.39	3.60	4.39	3.58	3.16	4.03	3.06	2.36	2.24	4.03	2.44	2.80	1.96	3.96
K_2O	3.20	3.23	1.17	1.85	2.49	1.30	4.18	1.17	1.19	1.28	2.95	6.26	5.92	5.11	5.54	2.10	8.7	3.18
P_2O_5	0.62	0.62	0.12	2.93	0.28	0.44	0.43	0.38	0.43	0.46	0.47	0.79	0.57	0.22	1.38	0.90	0.89	0.37
LOI	2.00	2.24	3.60	2.93	3.99	1.50	1.25	3.40	2.10	2.29	2.38	1.11	1.39	4.65	1.94	0.95	3.81	1.02
Total	100.87	100.70	99.29	99.22	104.66	103.79	100.90	101.00	104.38	104.89	99.61	100.10	101.10	99.15	99.51	100.70	100.8	99.04
Sr	913.00	982.00	828.00	797.00	406.00	638.00	551.00	717.00	674.00	971.00	526.00	633.00	517.00	591.00	2161.00	627.00	751.00	1002.2
Ba	1209.0	1204.0	483.0	844.5	380.0	615.0	694.0	614.0	835.0	785.0	1180.0	650.0	459.0	1233.0	1330.0	2000.0	803.0	1416.0
Rb	107.00	107.00	21.00	62.80	136.00	36.20	112.00	80.30	60.30	94.90	155.70	243.00	257.00	193.00	128.00	15.00	372.00	120.30
Ni	114.0	113.0	197.0	156.4	84.0	106.0	10.0	120.0	101.0	67.0	13.1	236.0	114.0	16.0	231.0	150.0	343.0	22.3
Co	31.0	28.0	29.0	27.5	25.0	32.0	21.0	33.0	31.0	34.0	33.2	n.d.	n.d.	n.d.	30.0	n.d.	n.d.	18.6
Cr	232	232	609	217.8	273	231	3	370	246	79	12	529	281	15	373	150	779	8
V	169.0	171.0	190.0	156.4	153.0	173.0	140.0	196.0	168.0	214.0	186.0	153.0	n.d.	86.0	173.0	200.0	178.0	152.0
Zr	277.0	271.0	60.0	167.4	263.0	153.0	229.0	176.0	155.0	242.0	199.0	1128.0	583.0	332.0	576.0	251.0	1049.0	311.0
Y	31.00	30.00	22.00	27.40	26.50	24.60	33.40	27.10	24.10	31.80	19.70	26.00	23.00	31.00	25.00	19.00	21.00	26.80
Nb	19.80	19.30	4.00	15.80	25.10	16.20	23.30	17.10	16.30	21.30	14.10	55.20	30.90	5.00	153.00	57.00	51.60	15.00
Ga	n.d.	n.d.	n.d.	18.7	n.d.	n.d.	n.d.	n.d.	n.d.	n.d.	17.1	22.0		n.d.	n.d.	n.d.	23.0	22.0
La	61.00	59.00	37.00	59.89	55.10	43.80	60.90	48.70	44.10	63.40	41.23	92.00	57.00	105.70	n.d.	n.d.	90.00	70.60
Ce	117.0	110.0	42	118.77	103	83.7	122	98	83.4	125	77.13	201	124	186	n.d.	n.d.	185	134.8
Pr	n.d.	n.d.	n.d.	13.16	11.50	9.76	14.10	11.80	9.77	15.30	7.64	n.d.	n.d.	18.20	n.d.	n.d.	n.d.	14.70
Nd	45.00	44.00		52.40	40.40	36.07	52.06	44.06	36.70	57.10	28.67	86.00	62.00	60.00	22.00	n.d.	76.00	55.80
Sm	n.d.	n.d.	n.d.	9.32	7.29	6.67	9.85	8.47	6.76	10.39	4.64	n.d.	n.d.	9.70	4.35	n.d.	n.d.	8.53
Eu	n.d.	n.d.	n.d.	2.54	1.62	1.79	2.37	2.18	1.83	2.65	1.20	n.d.	n.d.	2.08	n.d.	n.d.	n.d.	1.91
Gd	n.d.	n.d.	n.d.	7.11	5.97	5.67	8.21	7.11	5.71	8.59	3.64	n.d.	n.d.	6.30	n.d.	n.d.	n.d.	6.09
Tb	n.d.	n.d.	n.d.	1.01	0.86	0.79	1.16	0.98	0.81	1.18	0.58	n.d.	n.d.	0.82	n.d.	n.d.	n.d.	0.88
Dy	n.d.	n.d.	n.d.	5.06	4.63	4.38	6.15	5.11	4.39	6.06	3.20	n.d.	n.d.	4.35	n.d.	n.d.	n.d.	4.68
Er	n.d.	n.d.	n.d.	2.31	2.45	2.31	3.08	2.46	2.31	2.89	1.69	n.d.	n.d.	2.20	n.d.	n.d.	n.d.	2.37
Tm	n.d.	n.d.	n.d.	0.38	n.d.	n.d.	n.d.	n.d.	n.d.	n.d.	0.30	n.d.	n.d.	0.31	n.d.	n.d.	n.d.	0.40
Yb	n.d.	n.d.	n.d.	2.13	2.33	2.11	2.77	2.18	2.11	2.53	1.74	n.d.	n.d.	2.06	n.d.	n.d.	n.d.	2.23
Lu	n.d.	n.d.	n.d.	0.33	0.348	0.315	0.421	0.327	0.314	0.375	0.270	n.d.	n.d.	0.330	n.d.	n.d.	n.d.	0.360
Hf	n.d.	n.d.	n.d.	3.5	5.10	3.04	4.90	3.96	2.97	5.67	2.17	n.d.	n.d.	4.26	n.d.	n.d.	n.d.	7.65
Cs	n.d.	n.d.	n.d.	6.1	n.d.	n.d.	n.d.	n.d.	n.d.	n.d.	6.70	n.d.	n.d.	8.15	n.d.	n.d.	n.d.	5.80
Pb	n.d.	n.d.	n.d.	n.d.	n.d.	14.65	n.d.	n.d.	14.39	10.13	n.d.	12.00	7.00	7.54	n.d.	n.d.	n.d.	n.d.
Ta	n.d	n.d.	5.00	0.98	1.52	0.93	1.38	1.00	0.94	1.24	1.28	n.d.	n.d.	1.20	n.d.	n.d.	n.d.	0.97
Th	7.00	18.00	15.00	10.10	25.37	11.72	18.28	13.86	11.39	16.45	21.57	21.00	10.00	91.80	n.d.	n.d.	21.00	38.14
U	n.d.	n.d.	2.00	2.68	5.66	2.65	5.42	3.12	2.55	3.87	6.10	n.d.	n.d.	16.66	n.d.	n.d.	n.d.	6.79
$^{87}Sr/^{86}Sr$	n.d.	n.d.	n.d.	0.7076	n.d.	0.7063	n.d.	0.7076	0.7064	0.7074	n.d.	n.d.	n.d.	n.d.	0.7036	n.d.	n.d.	n.d.
$^{143}Nd/^{144}Nd$	n.d.	n.d.	n.d.	0.5125	n.d.	n.d.	n.d.	n.d.	n.d.	n.d.	n.d.	n.d.	n.d.	n.d.	0.5128	n.d.	n.d.	n.d.

Sources: Data taken from (1) Seyitoğlu et al. (1997); (2) Ercan et al. (1985); (3) Aldanmaz et al. (2000); (4) Ercan et al. (1995); (5) Guleç (1991).
Note: n.d.—not determined.

TABLE 4. REPRESENTATIVE CHEMICAL ANALYSES OF THE ALKALINE GROUP FROM WESTERN ANATOLIA

Sample no.	64-Qkv2-9	TM-9-57	106064	TM-84-1	TM-9-212	106065	TM-9-67	K-93-62	K-93-63	K-93-64	K-92-3	K-92-5	K-92-8	K-93-65	K-93-56	K-93-50	K-93-68	K-93-71	K-93-78
Source of data	1	1	1	1	1	1	1	2	2	2	2	2	2	2	2	2	2	2	2
SiO_2	45.48	46.10	46.30	47.20	47.53	47.76	48.43	45.72	47.80	46.20	48.39	48.46	45.74	45.20	47.61	44.94	47.53	47.04	37.1
TiO_2	2.19	1.95	1.94	1.89	1.89	1.77	1.89	2.22	1.78	2.20	1.84	1.90	2.43	2.04	1.89	2.23	1.80	1.92	3.55
Al_2O_3	16.61	16.96	17.25	17.91	18.13	17.93	18.08	18.33	18.08	18.32	18.22	18.49	16.75	16.96	18.16	16.80	17.81	17.52	13.61
Fe_2O_3	10.12	9.04	9.03	8.33	8.25	8.02	8.52	9.20	8.03	8.75	8.29	8.27	10.45	9.11	8.37	9.84	8.10	8.26	9.85
MnO	0.170	0.180	0.150	0.150	0.140	0.150	0.170	0.150	0.140	0.140	0.140	0.140	0.160	0.160	0.160	0.157	0.139	0.141	0.122
MgO	6.08	7.00	7.31	6.88	5.57	6.02	4.87	4.57	5.82	4.60	5.90	5.59	5.93	6.68	4.59	6.05	6.04	5.64	10.91
CaO	10.49	9.12	8.88	8.49	7.81	7.68	7.99	8.89	7.84	8.90	7.85	7.87	10.72	9.51	7.97	10.53	8.20	8.54	14.61
Na_2O	4.31	6.15	5.17	5.35	6.02	5.85	6.50	5.29	5.61	5.01	5.66	5.74	4.49	5.98	6.08	4.81	5.39	5.22	2.59
K_2O	1.95	1.72	3.18	3.24	3.75	3.73	1.82	3.13	3.62	3.11	3.61	3.63	2.54	1.69	3.18	2.34	3.50	3.23	1.91
P_2O_5	1.18	1.12	1.14	0.84	0.86	0.80	0.79	1.05	0.81	0.79	0.81	0.78	1.06	1.16	0.79	1.21	0.82	0.72	3
LOI	1.49	0.74	0.00	0.03	0.00	0.13	1.04	0.29	0.17	1.30	0.16	0.35	0.20	0.43	0.21	0.31	0.16	0.30	0.73
Total	100.08	100.07	100.36	100.29	99.94	99.86	100.10	98.80	99.40	99.30	100.60	101.20	100.50	98.9	98.6	99.2	99.2	98.5	98.0
Sr	1585.0	1146.0	1136.0	912.0	1016.0	913.0	953.0	1149.3	889.8	946.1	896.9	881.8	1195.6	1160.2	887.2	1262.1	899.8	853.1	1248.2
Ba	995.0	1035.0	948.0	820.0	921.0	846.0	837.0	858.6	869.4	714.9	856.9	896.7	830.6	999.0	771.3	937.9	834.4	829.6	679.4
Rb	27.0	64.0	72.0	76.0	78.0	81.0	58.0	85.9	80.1	60.6	83.2	81.3	47.5	49.6	76.9	54.2	77.0	87.5	19.4
Ni	34.0	69.0	78.0	72.0	47.0	70.0	34.0	13.1	63.4	19.0	77.4	55.2	46.8	60.7	31.9	40.0	65.0	43.1	82.1
Co	38.0	28.0	35.0	31.0	28.0	30.0	25.0	33.9	32.2	32.8	27.2	33.2	35.5	38.0	38.7	39.3	37.9	34.9	50.0
Cr	39.0	89.0	94.0	80.0	50.0	56.0	39.0	4.5	54.2	21.4	144.4	63.0	157.7	72.4	39.4	51.4	57.2	76.2	154.4
V	228.0	201.0	206.0	194.0	182.0	170.0	165.0	157.1	130.5	162.9	141.4	136.3	195.2	170.9	138.2	192.0	141.7	156.9	262.8
Zr	242.0	236.0	241.0	217.0	256.0	225.0	275.0	281.0	251.0	250.0	256.0	252.0	265.0	279.0	299.0	261.9	256	254.5	250.5
Y	31.0	29.0	27.0	26.0	28.0	25.0	26.0	30.3	25.6	25.4	25.4	27.8	28.3	28.5	27.7	30.6	26.7	27.7	36.7
Nb	116.0	103.0	103.0	88.0	102.0	92.0	100.0	97.6	99.6	86.8	99.7	98.8	86.3	110.0	104.4	92.6	97.1	94.9	67.3
Ga	n.d	n.d	n.d	n.d	n.d	n.d	n.d	27.0	22.1	26.8	24.5	22.9	25.3	24.8	25.7	24.6	23.3	24.9	25.0
La	n.d	n.d	n.d	n.d	n.d	n.d	n.d	n.d	n.d	n.d	n.d	n.d	n.d	62.30	46.20	74.10	49.40	47.80	61.94
Ce	n.d	n.d	n.d	n.d	n.d	n.d	n.d	n.d	n.d	n.d	n.d	n.d	n.d	123.00	82.40	134.80	92.50	90.10	136.04
Pr	n.d	n.d	n.d	n.d	n.d	n.d	n.d	n.d	n.d	n.d	n.d	n.d	n.d	11.60	9.30	14.60	8.49	9.70	16.23
Nd	61.45	40.29	47.38	35.54	9.62	37.17	38.19	n.d	n.d	n.d	n.d	n.d	n.d	48.30	34.50	55.60	36.40	38.10	66.35
Sm	10.621	7.300	8.412	6.615	7.080	6.920	7.010	n.d	n.d	n.d	n.d	n.d	n.d	8.200	6.600	9.400	6.300	7.300	12.480
Eu	n.d	n.d	n.d	n.d	n.d	n.d	n.d	n.d	n.d	n.d	n.d	n.d	n.d	2.53	2.10	2.90	1.95	2.20	3.61
Gd	n.d	n.d	n.d	n.d	n.d	n.d	n.d	n.d	n.d	n.d	n.d	n.d	n.d	6.81	5.20	7.80	5.59	10.00	9.56
Tb	n.d	n.d	n.d	n.d	n.d	n.d	n.d	n.d	n.d	n.d	n.d	n.d	n.d	n.d	n.d	n.d	n.d	n.d	n.d
Dy	n.d	n.d	n.d	n.d	n.d	n.d	n.d	n.d	n.d	n.d	n.d	n.d	n.d	5.41	4.20	5.50	4.66	4.80	6.05
Er	n.d	n.d	n.d	n.d	n.d	n.d	n.d	n.d	n.d	n.d	n.d	n.d	n.d	2.63	2.20	2.50	2.33	2.60	2.69
Tm	n.d	n.d	n.d	n.d	n.d	n.d	n.d	n.d	n.d	n.d	n.d	n.d	n.d	n.d	n.d	n.d	n.d	n.d	n.d
Yb	n.d	n.d	n.d	n.d	n.d	n.d	n.d	n.d	n.d	n.d	n.d	n.d	n.d	2.34	2.30	2.30	2.17	2.30	1.92
Lu	n.d	n.d	n.d	n.d	n.d	n.d	n.d	n.d	n.d	n.d	n.d	n.d	n.d	0.35	0.30	0.30	0.34	0.30	0.29
Hf	n.d	n.d	n.d	n.d	n.d	n.d	n.d	n.d	n.d	n.d	n.d	n.d	n.d	n.d	4.7	4.6	n.d	5.0	n.d.
Cs	n.d	n.d	n.d	n.d	n.d	n.d	n.d	n.d	n.d	n.d	n.d	n.d	n.d	n.d	0.58	0.6	n.d	0.82	n.d.
Pb	10	11	10	10	7	9	9	n.d	n.d	n.d	n.d	n.d	n.d	n.d	3.1	7	n.d	5.9	n.d.
Ta	n.d	n.d	n.d	n.d	n.d	n.d	n.d	n.d	n.d	n.d	n.d	n.d	n.d	n.d	5.60	5.30	n.d	6.00	4.06
Th	n.d	n.d	n.d	n.d	n.d	n.d	n.d	n.d	n.d	n.d	n.d	n.d	n.d	n.d	7.00	9.40	n.d	9.20	2.77
U	n.d	n.d	n.d	n.d	n.d	n.d	n.d	n.d	n.d	n.d	n.d	n.d	n.d	n.d	1.9	2.1	n.d	2.1	n.d.
$^{87}Sr/^{86}Sr$	0.7035	0.7033	0.7032	0.7031	0.7031	0.7032	0.7033	n.d.	n.d.	n.d.	n.d.	n.d.	n.d.	0.7033	0.7031	0.7034	0.7032	0.7033	0.7032
$^{143}Nd/^{144}Nd$	0.51285	0.51292	0.51290	0.51300	0.51295	0.51300	0.51290	n.d.	n.d.	n.d.	n.d.	n.d.	n.d.	0.51290	0.51290	0.51280	0.51290	0.51290	0.51290
$^{0206}Pb/^{204}Pb$	n.d.	n.d.	n.d.	n.d.	n.d.	n.d.	n.d.	n.d.	n.d.	n.d.	n.d.	n.d.	n.d.	18.860	18.904	18.873	18.689	18.816	18.890
$^{207}Pb/^{204}Pb$	n.d.	n.d.	n.d.	n.d.	n.d.	n.d.	n.d.	n.d.	n.d.	n.d.	n.d.	n.d.	n.d.	15.622	15.614	15.646	15.621	15.642	15.635
$^{208}Pb/^{204}Pb$	n.d.	n.d.	n.d.	n.d.	n.d.	n.d.	n.d.	n.d.	n.d.	n.d.	n.d.	n.d.	n.d.	38.664	38.648	38.839	38.560	38.770	38.764

Sample no.	K-93-80	K-93-91	K-93-67	K-93-81	K-93-82	K-93-84	K-93-85	K-93-86	6	TM-80-819	EA270	TM-80-819	EA270	EA267	EA82B	14	EA260
Source of data	2	2	2	2	2	2	2	2	3	1	4	1	4	4	4	5	4
SiO_2	44.60	46.09	47.77	46.83	46.39	46.16	46.30	46.87	49.70	52.26	41.81	52.26	41.81	42.61	43.04	41.44	42.75
TiO_2	2.16	2.26	1.79	1.85	1.97	2.20	1.94	2.48	1.63	1.13	3.14	1.13	3.14	3.15	3.14	3.06	3.09
Al_2O_3	16.69	16.56	17.90	17.99	17.82	18.23	17.75	16.84	12.21	11.86	12.26	11.86	12.26	13.04	12.97	12.60	12.87
Fe_2O_3	9.94	9.61	8.08	8.27	8.48	8.73	8.40	8.60	7.27	5.57	14.38	5.57	14.38	14.24	14.11	13.77	14.30
MnO	0.164	0.173	0.143	0.150	0.150	0.142	0.149	0.132	0.120	0.100	0.22	0.10	0.22	0.22	0.22	0.22	0.21
MgO	5.68	6.99	6.12	5.94	6.15	4.57	5.99	6.53	7.77	6.75	7.74	6.75	7.74	7.98	8.05	7.82	8.19
CaO	10.69	9.35	7.94	8.20	8.68	8.94	8.62	9.11	8.70	10.73	11.03	10.73	11.03	11.06	10.97	10.77	10.91
Na_2O	4.86	4.76	5.48	5.65	5.49	4.75	5.54	4.75	2.75	2.61	5.33	2.61	5.33	4.62	4.74	4.71	4.33
K_2O	2.32	2.82	3.50	3.55	3.45	2.99	3.40	3.08	4.84	5.04	1.52	5.04	1.52	1.97	1.43	1.56	1.42
P_2O_5	1.15	0.73	0.79	0.78	0.86	0.80	0.84	0.94	1.72	1.29	1.25	1.29	1.25	1.29	1.26	1.25	0.99
LOI	0.81	0.16	0.13	0.27	0.13	1.52	0.02	0.42	2.32	2.41	1.27	2.41	1.27	2.44	2.72	1.44	1.57
Total	99.1	99.2	99.4	98.9	99.3	99	98.9	99.8	99.05	99.76	99.19	99.76	99.19	100.18	99.94	98.64	99.07
Sr	1381.4	943	894.2	902.5	925.4	909.2	917.6	829.3	2169.0	2995.0	1077.4	2995.0	1077.4	1131.1	1073.1	1060.0	908.3
Ba	990.7	916.9	848.3	873.0	870.9	807.8	817.1	757.1	1466.0	2143.0	682.5	2143.0	682.5	645.2	652.2	688.0	511.5
Rb	52.9	61.6	79.1	78.9	73.7	75.5	76.3	67.6	105.0	119.0	21.3	119.0	21.3	23.2	33.5	31.0	17.3
Ni	33.7	79.4	70.0	59.4	57.3	64.1	61.0	50.8	235.0	80.0	70.4	80.0	70.4	69.3	57.5	40.0	104.5
Co	36.3	39.7	34.0	37.4	42.3	32.9	37.1	50.5	40.0	24.0	47.2	24.0	47.2	46.3	39.2	n.d.	50.9
Cr	45.5	109.2	71.3	68.7	57.7	74.5	68.4	37.5	284.0	273.0	92.1	273.0	92.1	82.8	77.0	70.0	137.3
V	210.0	185.2	138.3	146.3	150.9	159.4	164.2	204	130.0	121.0	206.2	121.0	206.2	206.0	221.8	150.0	211.3
Zr	285.0	262.0	250.5	249	248.4	250.0	254.7	249.4	466.0	369.0	364.8	369.0	364.8	376.8	364.7	356.0	314.1
Y	30.1	28.3	25.5	24.5	26.3	26.9	27.0	33.4	37.0	22.00	35.4	22.00	35.4	37.0	35.1	31.0	31.5
Nb	116.3	84.8	98.2	99.1	97.7	99.8	96.8	79.7	91.0	66.0	101.2	66.0	101.2	104.8	100.3	102.0	83.9
Ga	22.9	25.1	22.3	24.0	23.7	22.4	24.0	26.6	n.d.	n.d.	24.0	n.d.	24.0	24.5	24.4	n.d.	23.2
La	72.60	49.40	47.40	48.50	53.30	n.d.	n.d.	n.d	164.00	n.d.	70.23	n.d.	70.23	71.97	67.82	68.20	54.65
Ce	138.10	94.00	87.00	89.80	96.10	n.d.	n.d.	n.d	262.00	n.d.	135.14	n.d.	135.14	138.25	130.06	138.00	107.47
Pr	14.50	9.47	8.21	8.43	9.90	n.d.	n.d.	n.d	n.d.	n.d.	15.58	n.d.	15.58	16.12	15.16	15.50	12.72
Nd	51.5	39.4	32.1	33.7	37.3	n.d.	n.d.	n.d	n.d.	111.68	65.62	111.68	65.62	67.91	64.36	51.40	54.85
Sm	8.90	7.21	5.92	6.17	7.30	n.d.	n.d.	n.d	n.d.	15.92	12.40	15.92	12.40	12.46	12.08	12.20	10.51
Eu	2.60	2.27	1.91	1.94	2.30	n.d.	n.d.	n.d	n.d.	n.d.	3.73	n.d.	3.73	3.72	3.62	3.70	3.20
Gd	6.40	6.47	5.36	5.53	6.00	n.d.	n.d.	n.d	n.d.	n.d.	10.17	n.d.	10.17	10.00	9.91	10.02	8.89
Tb	n.d.	n.d.	n.d.	n.d.	n.d.	n.d.	n.d.	n.d	n.d.	n.d.	1.47	n.d.	1.47	1.47	1.43	1.37	1.30
Dy	4.80	5.11	4.27	4.46	4.40	n.d.	n.d.	n.d	n.d.	n.d.	7.33	n.d.	7.33	7.44	7.17	7.23	6.46
Er	2.30	2.66	2.35	2.26	2.30	n.d.	n.d.	n.d	n.d.	n.d.	2.94	n.d.	2.94	3.01	2.92	3.04	2.62
Tm	n.d	n.d.	n.d	n.d	n.d	n.d.	n.d.	n.d	n.d.	n.d.	0.45	n.d.	0.45	0.46	0.45	0.38	0.40
Yb	2.00	2.35	2.16	2.14	2.10	n.d.	n.d.	n.d	n.d.	n.d.	2.37	n.d.	2.37	2.33	2.34	2.21	2.07
Lu	0.30	0.33	0.31	0.31	0.30	n.d.	n.d.	n.d	n.d.	n.d.	0.34	n.d.	0.34	0.34	0.33	0.28	0.29
Hf	4.10	n.d.	n.d.	n.d.	4.50	n.d.	n.d.	n.d	n.d.	n.d.	7.91	n.d.	7.91	7.79	7.73	7.93	6.99
Cs	0.49	n.d.	n.d.	n.d.	0.64	n.d.	n.d.	n.d	n.d.	n.d.	0.80	n.d.	0.80	0.70	0.90	0.75	0.50
Pb	6.10	n.d.	n.d.	n.d.	4.10	n.d.	n.d.	n.d	22.00	22.00	11.90	22.00	11.90	6.70	7.00	4.55	8.00
Ta	5.20	n.d.	n.d.	n.d.	5.80	n.d.	n.d.	n.d	6.00	n.d.	6.68	n.d.	6.68	6.56	6.57	6.53	5.65
Th	8.60	n.d.	n.d.	n.d.	8.00	n.d.	n.d.	n.d	29.00	n.d.	9.10	n.d.	9.10	9.26	9.17	8.53	7.22
U	2.00	n.d.	n.d.	n.d.	1.80	n.d.	n.d.	n.d	29.00	n.d.	2.91	n.d.	2.91	3.35	2.96	2.65	2.32
$^{87}Sr/^{86}Sr$	0.7033	0.7032	0.7031	0.7030	0.7030	n.d.	n.d.	n.d.	n.d.	0.7035	0.7031	0.7035	0.7031	n.d.	n.d.	0.7031	n.d.
$^{143}Nd/^{144}Nd$	0.5128	0.5129	0.5129	0.5129	0.5129	n.d.	n.d.	n.d.	n.d.	0.5127	0.5130	0.5127	0.5130	n.d.	n.d.	0.5129	n.d.
$^{206}Pb/^{204}Pb$	19.064	18.799	18.708	18.795	18.819	n.d.	n.d.	n.d.	n.d.	n.d.	n.d.	n.d.	n.d.	n.d.	n.d.	n.d.	n.d.
$^{207}Pb/^{204}Pb$	15.683	15.633	15.630	15.607	15.612	n.d.	n.d.	n.d.	n.d.	n.d.	n.d.	n.d.	n.d.	n.d.	n.d.	n.d.	n.d.
$^{208}Pb/^{204}Pb$	39.113	38.679	38.584	38.593	38.622	n.d.	n.d.	n.d.	n.d.	n.d.	n.d.	n.d.	n.d.	n.d.	n.d.	n.d.	n.d.

(continued)

TABLE 4. *Continued*

Sample no.	5	EA254	TE-14	48	49	46	47	44	45	41	4	EA262	EA415	TE-41	EA249	EA253
Source of data	5	4	6	7	7	7	7	7	7	7	7	4	4	6	4	4
SiO_2	38.74	45.69	41.44	45.00	44.14	45.14	45.13	41.99	43.27	46.39	47.17	46.99	46.07	46.39	49.97	50.52
TiO_2	2.82	2.78	3.06	2.75	2.83	2.84	2.93	3.22	2.90	2.84	2.56	2.82	2.83	2.84	2.58	2.59
Al_2O_3	11.87	13.29	12.60	12.36	12.36	12.72	12.58	12.45	12.18	12.87	13.19	13.01	13.21	12.87	14.30	14.62
Fe_2O_3	13.75	12.13	13.77	11.22	11.43	11.47	12.10	13.58	11.90	12.21	11.16	12.22	12.04	12.21	10.69	10.63
MnO	0.26	0.17	0.22	0.16	0.16	0.15	0.16	0.20	0.17	0.17	0.15	0.18	0.16	0.17	0.14	0.13
MgO	8.3	9.62	7.82	8.96	9.47	8.02	8.49	7.95	9.64	8.47	8.25	8.38	9.25	8.47	6.90	6.89
CaO	12.77	9.96	10.77	10.62	10.46	10.84	10.84	10.49	10.85	9.83	9.95	10.76	10.91	9.83	8.74	8.90
Na_2O	3.86	4.25	4.71	3.95	3.37	4.26	3.54	4.99	3.92	3.02	2.98	3.49	3.14	3.02	3.51	3.57
K_2O	1.19	1.37	1.56	1.71	1.61	1.80	1.05	1.69	1.00	1.57	1.61	1.67	1.51	1.57	1.63	1.63
P_2O_5	1.64	0.79	1.25	0.88	0.94	0.94	1.07	1.26	1.07	0.72	0.62	0.74	0.76	0.72	0.49	0.49
LOI	3.16	1.27	1.44	1.36	2.79	1.08	1.68	2.02	2.91	1.37	1.89	1.86	2.83	1.37	1.46	1.62
Total	98.36	100.05	98.64	98.97	99.56	99.26	99.57	99.84	99.81	99.46	99.53	100.25	99.88	99.46	98.95	99.97
Sr	1382.0	1015.2	1060.0	853.0	856.0	856.0	950.0	1220.0	972.0	823.0	846.0	788.6	728.6	823.0	505.9	487.3
Ba	746.0	415.8	688.0	540.0	467.0	601.0	510.0	667.0	512.0	397.0	1092.0	469.5	418.6	397.0	245.0	230.0
Rb	30.0	16.5	31.0	19.0	16.0	26.0	2.0	11.0	6.0	19.0	26.0	21.7	24.1	19.0	17.9	18.3
Ni	40.0	142.3	40.0	100.0	100.0	70.0	151.0	83.0	182.0	70.0	150.0	156.0	168.6	70.0	176.9	183.3
Co	n.d.	47.9	n.d.	n.d.	n.d.	n.d.	n.d.	n.d.	n.d.	n.d.	n.d.	46.8	47.7	n.d.	35.4	38.0
Cr	40.0	194.6	70.0	700.0	400.0	700.0	282.0	108.0	254.0	150.0	300.0	239.2	228.5	150.0	278.6	276.3
V	100.0	200.8	150.0	150.0	70.0	100.0	225.0	224.0	226.0	<40.0	100.0	203.2	208.5	40.0	200.4	201.0
Zr	361.0	267.4	356.0	272.0	283.0	284.0	310.0	406.0	317.0	259.0	218.0	264.9	246.5	259.0	185.3	193.6
Y	36.0	27.7	31.0	24.0	26.0	25.0	27.0	27.0	27.0	24.0	23.0	27.3	25.8	24.0	21.3	22.2
Nb	114.0	69.2	102.0	73.0	77.0	75.0	86.0	108.0	87.0	61.0	47.0	59.6	62.5	61.0	31.9	33.8
La	n.d.	38.68	68.20	44.50	n.d.	n.d.	n.d.	n.d.	n.d.	36.60	29.90	36.92	37.26	36.60	20.00	20.86
Ce	n.d.	79.27	138.00	90.00	n.d.	n.d.	n.d.	n.d.	n.d.	74.00	63.00	73.49	74.02	74.00	42.86	44.54
Pr	n.d.	9.34	15.50	10.60	n.d.	n.d.	n.d.	n.d.	n.d.	8.90	7.40	8.98	8.79	8.90	5.57	5.73
Nd	n.d.	39.59	61.40	42.80	n.d.	n.d.	n.d.	n.d.	n.d.	36.90	31.00	39.79	39.10	36.90	25.36	26.77
Sm	n.d.	8.29	12.20	8.90	n.d.	n.d.	n.d.	n.d.	n.d.	8.30	6.90	8.13	8.08	8.30	6.01	6.05
Eu	n.d.	2.57	3.70	2.89	n.d.	n.d.	n.d.	n.d.	n.d.	2.71	2.24	2.56	2.52	2.71	1.94	1.99
Gd	n.d.	7.39	10.02	7.40	n.d.	n.d.	n.d.	n.d.	n.d.	7.43	6.23	7.08	7.31	7.43	5.85	5.63
Tb	n.d.	1.09	1.37	1.01	n.d.	n.d.	n.d.	n.d.	n.d.	0.99	0.86	1.07	1.06	0.99	0.85	0.85
Dy	n.d.	5.46	7.23	5.44	n.d.	n.d.	n.d.	n.d.	n.d.	5.47	4.77	5.52	5.33	5.47	4.35	4.53
Er	n.d.	2.23	3.04	2.25	n.d.	n.d.	n.d.	n.d.	n.d.	2.44	2.13	2.21	2.16	2.44	1.78	1.83
Tm	n.d.	0.34	0.38	0.28	n.d.	n.d.	n.d.	n.d.	n.d.	0.31	0.26	0.35	0.33	0.31	0.28	0.28
Yb	n.d.	1.83	2.21	1.50	n.d.	n.d.	n.d.	n.d.	n.d.	1.68	1.51	1.79	1.71	1.68	1.47	1.47
Lu	n.d.	0.26	0.28	0.23	n.d.	n.d.	n.d.	n.d.	n.d.	0.28	0.22	0.26	0.25	0.28	0.21	0.22
Hf	n.d.	5.88	7.93	6.13	n.d.	n.d.	n.d.	n.d.	n.d.	6.08	4.98	5.57	5.52	6.08	4.34	4.40
Cs	n.d.	3.60	0.75	0.39	n.d.	n.d.	n.d.	n.d.	n.d.	0.73	2.67	0.30	1.20	0.73	1.70	2.70
Pb	n.d.	8.90	5.00	3.61	n.d.	n.d.	n.d.	n.d.	n.d.	3.03	3.18	4.30	1.40	3.00	8.70	1.20
Ta	n.d.	4.46	6.53	4.57	n.d.	n.d.	n.d.	n.d.	n.d.	3.96	3.09	3.79	4.04	3.96	2.11	2.16
Th	n.d.	5.74	8.53	6.36	n.d.	n.d.	n.d.	n.d.	n.d.	4.66	3.90	4.77	5.21	4.66	2.63	2.66
U	n.d.	1.90	2.65	1.82	n.d.	n.d.	n.d.	n.d.	n.d.	1.29	1.09	1.61	1.13	1.29	0.70	0.55
$^{87}Sr/^{86}Sr$	0.7030	n.d.	0.7031	0.7033	0.7032	0.7032	n.d.	n.d.	n.d.	0.7031	0.7033	n.d.	n.d.	0.7031	0.7033	n.d
$^{143}Nd/^{144}Nd$	0.51300	n.d.	0.51290	0.51290	0.51293	0.51293	n.d.	n.d.	n.d.	0.51310	0.51290	n.d.	n.d.	0.51290	0.51290	n.d

Sources: Data taken from (1) Güleç (1991); (2) Alıcı et al. (2002); (3) Ercan et al. (1985); (4) Aldanmaz et al. (2000); (5) Ercan et al. (1990); (6) Yılmaz et al. (2001); (7) Ercan et al. (1995).

Note: n.d.—not determined.

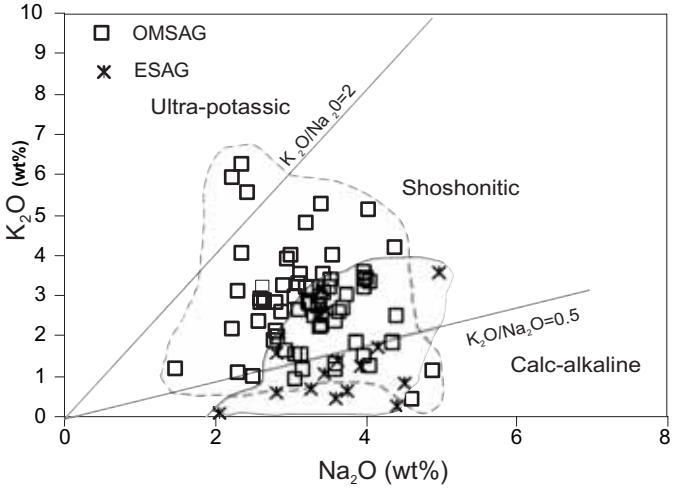

Figure 4. K_2O versus Na_2O diagram of the Eocene subalkaline group (ESAG) and Oligocene–early Miocene subalkaline group (OMSAG) lavas using the classification scheme of Peccerillo and Taylor (1976).

(15–19 wt%), and are either shoshonitic or high-K calc-alkaline on a K_2O versus Na_2O plot (Fig. 4), with only four samples falling in the ultrapotassic field. In the AFM diagram (not shown here), they display a calc-alkaline trend. Their MgO contents range from 1 to 10 wt%. Variations between the MgO and major-element contents such as SiO_2, CaO, Fe_2O_3, and Al_2O_3 of the Oligocene—early Miocene and ESAG rocks are similar, although ESAG lavas appear to have lower MgO contents (0.70–6.23 wt%) (Fig. 5).

The calc-alkaline nature of the OMSAG rocks is also evident from their trace-element concentrations and interelement relationships. These rocks are strongly depleted in highly compatible (Ni = 3–167 ppm, Cr = 4.5–400 ppm) to moderately compatible (TiO_2 = 0.5–1 wt%) elements with respect to the MORB, but moderately to strongly enriched in highly incompatible elements (Ba = 132–2000 ppm, Th = 11–52 ppm, La = 30–92 ppm), yielding high Th/Yb (5–24) and Zr/Y (4–11) ratios. These features collectively indicate derivation from moderately to strongly evolved melts (cf. Frey et al., 1978).

In MORB-normalized multielement diagrams (Fig. 6), the OMSAG lavas display enrichment trends in the most incompatible elements (Ba, Rb, Th, K, La, and Ce) and negative anomalies in Nb, Ta, P, and Ti. They are strongly enriched in LILE and LREE compared to the ESAG lavas and to island arc calc-alkaline basalts. Their chondrite-normalized REE patterns (Fig. 7) show enrichment in LREE, flat HREE (La/Sm_n = 3.31–6.60, Gd/Yb_n = 1.4–3.5, and La/Yb_n = 8–29), and minor negative Eu anomalies. All these geochemical characteristics indicate that the OMSAG rocks have similar multielement patterns to those of the ESAG, defining a subduction zone–related magmatic signature for their origin (McDonough, 1990; McCulloch and Gamble, 1991; Thirwall et al., 1994; Pearce and Peate, 1995).

Mildly Alkaline Group. The MAG is represented by basalt, trachy basalt, basaltic trachy andesite, trachy andesite, and trachyte (Fig. 3). The SiO_2 contents of these rocks range from 46 to 60 wt%, and they are commonly mildly silica-undersaturated. The maximum MgO and Ni contents of the mafic rocks (8 wt% and 100–150 ppm, respectively), combined with their Mg # (<60) [MgO/(MgO × 0.8 + FeO total)], imply that none of these lavas represents primary mantle-derived magma. This group is also characterized by moderate to high Al_2O_3 values, with TiO_2 contents ranging from ~1 wt% to 2 wt%, and by relatively high K_2O values for lower SiO_2 contents.

The differences between the alkaline and calc-alkaline mafic rocks are not significant, and both have similar values of Al_2O_3, TiO_2, Fe_2O_3, and CaO for a given SiO_2 content (not shown here), although mildly alkaline rocks extend to lower SiO_2 contents (46 wt% as opposed to 51 wt% in calc-alkaline lavas). All of these elements decrease as the SiO_2 content increases in both lineages, with the exception of Al_2O_3, which increases along with SiO_2. The only noteworthy difference between the samples following an alkaline trend and those with calc-alkaline characteristics is that the former have slightly higher Na_2O and significantly higher K_2O values at a given SiO_2 content (not shown here).

MAG lavas and SAG lavas (ESAG and OMSAG) show similar trends in MgO covariation diagrams (Fig. 5), and the MAG rocks form arrays between the AG and the OMSAG, indicating their transitional character (Fig. 5). The Ni and MgO abundances (up 10 wt%) in the most primitive MAG samples are rather high, and most basaltic samples of the MAG and AG with >4 wt% MgO follow the olivine-clinopyroxene fractionation trajectory defined by Hart and Davis (1978; Fig. 5).

When compared to the normalized multielement diagrams of the SAG lavas (ESAG and OMSAG), the MAG lavas have rather uniform compositions and display less marked enrichment trends in Ba, Th, and K and weaker negative P and Nb anomalies (Fig. 8). The Ti anomaly is also less apparent in the MAG rocks, and their Ba/Nb ratios (11–94) are also slightly lower. The REE patterns of the mildly alkaline lavas exhibit enrichment in LREE, but their $(La/Yb)_n$ ratios, which range between 9 and 17 (Fig. 7), are lower than those of the SAG lavas.

Alkaline Group. The AG lavas plot in the tephrite, basanite, phonotephrite, and foidite fields in the SiO_2 versus Na_2O+K_2O diagram (Fig. 3; Le Bas et al., 1986). These mafic lavas are TiO_2-rich (1.6–3.5 wt%), and their SiO_2 contents range from 41 to 48 wt%, which is significantly lower than those of the SAG and MAG. The AG and MAG rocks show similar correlations in MgO variation diagrams. They have rather uniform compositions, with high MgO and low SiO_2 contents.

The multielement patterns (Fig. 6) of rocks in this group are typical of ocean island basalts (OIB), with maximum enrichment in Nb. The chondrite-normalized REE patterns (Fig. 7) show that the AG lavas are highly enriched in LREE and that their $(La/Yb)_n$ ratios vary from 9 to 20, which is within the same range as in the SAG lavas with more basic compositions.

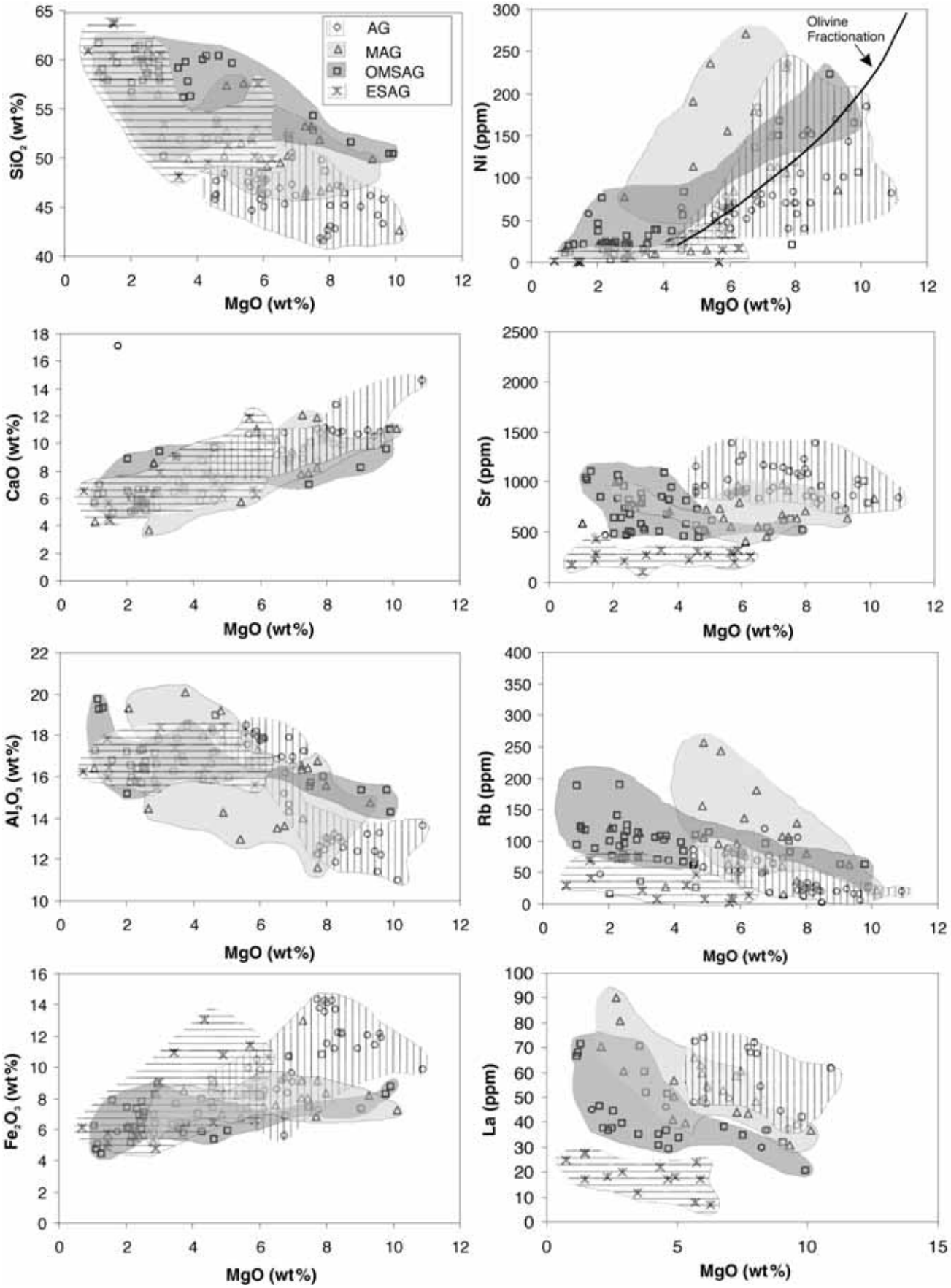

Figure 5. Selected major- and trace-element versus MgO variation diagrams for the Eocene subalkaline group (ESAG), Oligocene–early Miocene subalkaline group (OMSAG), mildly alkaline group (MAG), and alkaline group (AG) lavas.

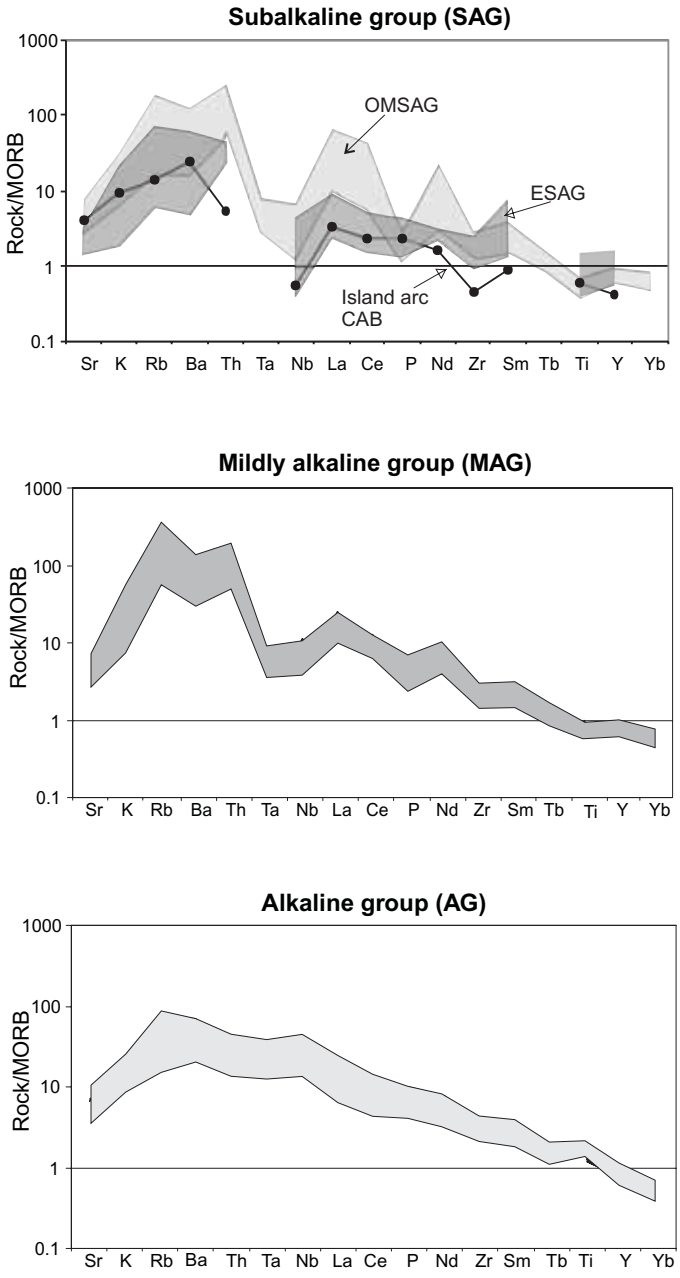

Figure 6. Mid-oceanic ridge basalt (MORB)-normalized multielement patterns for the subalkaline group (the Eocene subalkaline group, or ESAG, and Oligocene–early Miocene subalkaline group, or OMSAG), mildly alkaline group, and alkaline group lavas. The MORB normalizing values are from Sun and McDonough (1989); the island arc calc-alkaline basalt values are from Pearce (1982).

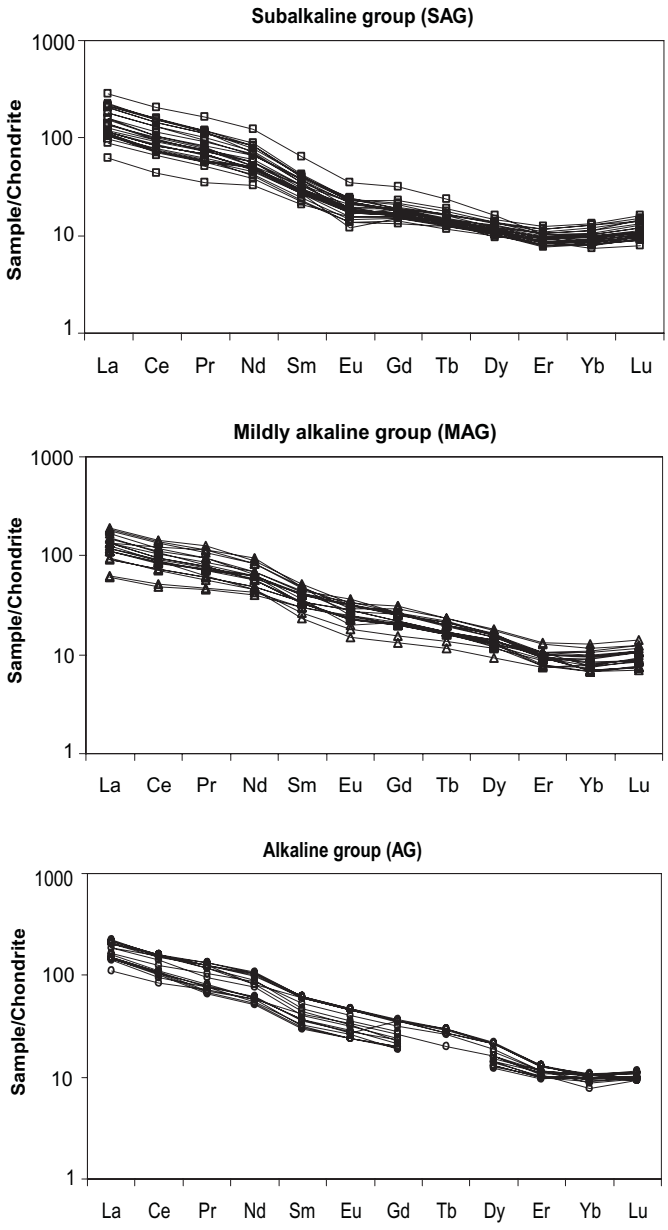

Figure 7. Chondrite-normalized rare earth element patterns for the subalkaline group (Eocene subalkaline group and Oligocene–early Miocene subalkaline group), mildly alkaline group, and alkaline group lavas. The chondrite normalizing values are from Boynton (1984).

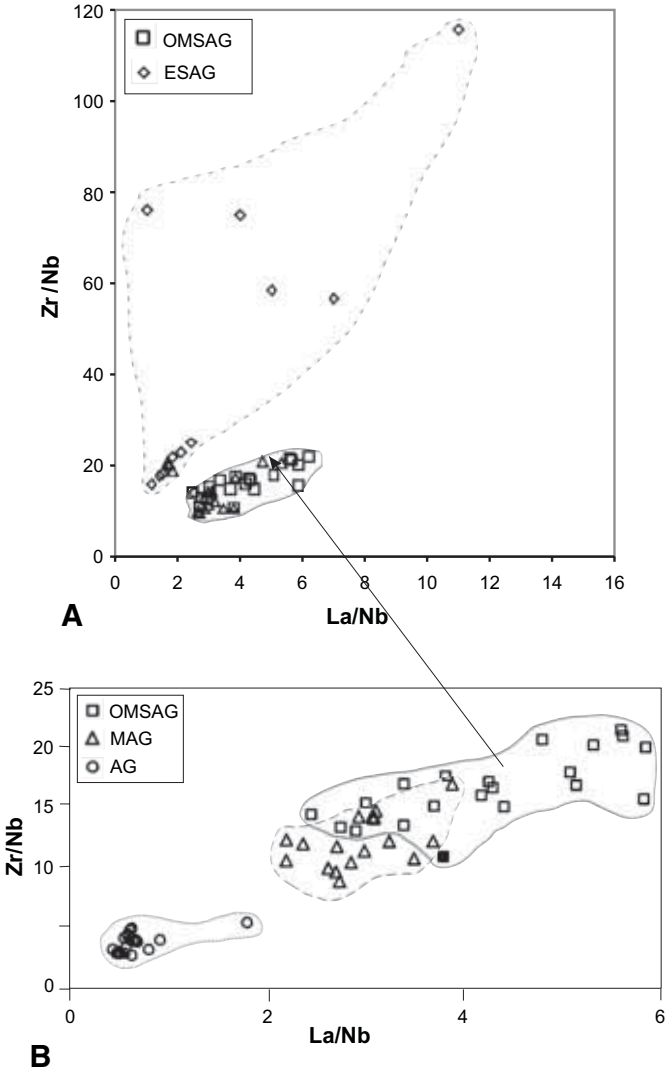

Figure 8. (A) Zr/Nb versus La/Nb diagram for the Eocene subalkaline group (ESAG) and Oligocene–early Miocene subalkaline group (OMSAG). (B) Zr/Nb versus La/Nb diagram for the Oligocene–early Miocene subalkaline group (OMSAG), mildly alkaline group (MAG), and alkaline group (AG) lavas.

The Zr/Nb versus La/Nb diagram clearly shows the geochemical distinction between the AG and the SAG and MAG (Fig. 8B). The MAG overlaps with the SAG, but its rocks have rather low La/Nb and Zr/Nb ratios compared to those of the SAG. The AG displays uniform compositions represented by the lowest La/Nb ratios compared to the other two groups.

Isotope Data

Figure 9, a ε_{Nd} (i) versus $^{87}Sr/^{86}Sr$ (i) diagram, shows the initial isotopic compositions of the three groups. Unfortunately, we have isotope data from only one ESAG sample. The SAG has the highest $^{87}Sr/^{86}Sr$ (i) (0.7087 to 0.7071) and the lowest ε_{Nd} (i) (–6.5 to –3.5) values. By contrast, the strongly AG has the lowest $^{87}Sr/^{86}Sr$ (i) (0.7033 to 0.7030) and the highest ε_{Nd} (i) (+6.5 to +2.5) values. The MAG has $^{87}Sr/^{86}Sr$ (i) values of 0.7075 to 0.7062 and ε_{Nd} (i) values of –3.6 to –1.6, falling between the SAG and strongly alkaline groups. These data indicate a transitional character of the MAG lavas that is supported by their major- and trace-element characteristics as well.

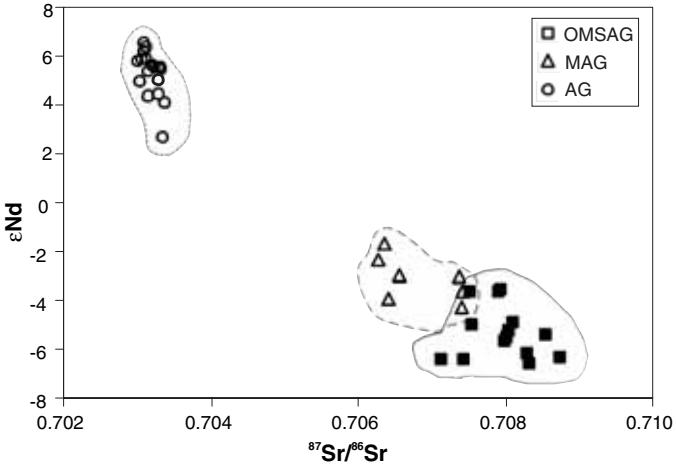

Figure 9. $\varepsilon Nd_{(i)}$, and $^{87}Sr/^{86}Sr$ diagram for the Oligocene–early Miocene subalkaline group (OMSAG), mildly alkaline group (MAG), and alkaline group (AG) lavas.

PETROGENESIS OF CENOZOIC VOLCANISM IN WESTERN ANATOLIA

Subalkaline Group

The least evolved ESAG and OMSAG lavas have similar geochemical features (major- and trace-element characteristics and interelement ratios), suggesting a common source for their parental magmas (Figs. 3–6). The compositions of the SAG (ESAG and OMSAG) lavas display a broad range, from moderately to highly evolved compositions, as evidenced by their MgO content (11–1 wt%). The majority of the SAG falls into either a shoshonitic or a high-K calc-alkaline field, with only four samples falling in the ultrapotassic field in a K_2O versus Na_2O diagram (Fig. 4), as defined by Peccerillo and Taylor (1976). The whole igneous province appears to have a potassic character (with K_2O/Na_2O ratios mostly between 0.5 and 2) that is consistent with the postcollisional nature of Cenozoic magmatism in western Anatolia.

The major- and trace-element trends in Figure 5 probably reflect the effects of both partial melting and fractionation processes. Some trace-element trends, such as the positive correlation between Ni and MgO, are probably fractionation related. Incompatible-element distributions show the negative

correlations with MgO expected from crystal fractionation. For example, the Rb and La values decrease with increasing MgO, and Sr shows a negative correlation with MgO within all individual groups (Fig. 5); however, the combined array shows a general decrease with decreasing MgO values, suggesting that there were apparent variations in the source and degree of melting trough time.

The presence of residual garnet in the source region is evident from the Gd/Yb (n) (1.5–3.2) and La/Yb (n) (10–50) ratios. Thirlwall et al. (1994) used the rare earth element (e.g., La/Yb) and HFSE (Nb/Zr) ratios to monitor the degree of partial melting in the generation of arc lavas. The La/Yb ratios are high and variable, and they increase with both La and Yb abundances (Figs. 10 and 11A). The low HREE abundances reflect the presence of residual garnet in the source region. Partial melting models show that steep trends in which La /Yb ratios vary from 10 to 50 can be produced only in the presence of residual garnet. Subsequent fractionation increases the La abundance, whereas the La/Yb ratio remains constant such that the flat trends generated by fractionation can be easily distinguished from steep partial melting trajectories. Figure 10 shows that the effects of partial melting were more important than fractional crystallization in controlling the compositional variations within the SAG lavas.

In MORB-normalized multielement diagrams (Fig. 6), the SAG (ESAG and OMSAG) lavas display enrichment trends in the most incompatible elements (Ba, Rb, Th, K, La, and Ce) and negative anomalies in Nb, Ta, P, and Ti. These are characteristics of magmas evolved at convergent margins, such as Andean-type calc-alkaline lavas (Thorpe et al., 1982; Davidson et al., 1991; Pearce and Peate, 1995). The fractionations of LILE/LREE, LILE/HFSE, and REE/HFSE (e.g., La/Nb, La/Yb, Zr/Nb, etc.) have been attributed to subduction-related metasomatism

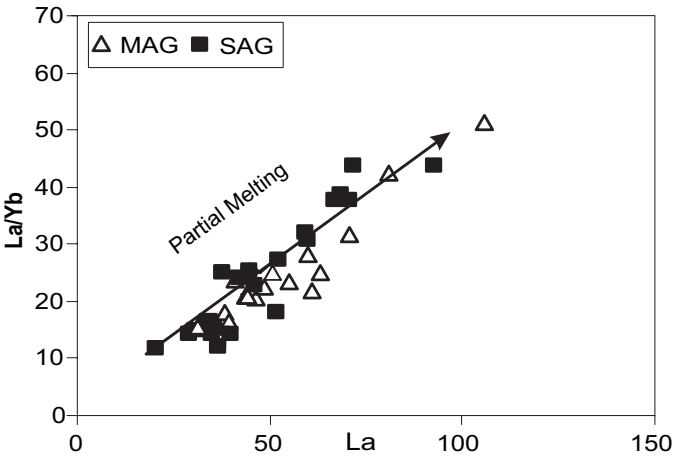

Figure 10. $(La/Yb)_n$ versus La (ppm) diagram for the mildly alkaline group (MAG) and subalkaline group (SAG) lavas illustrating the effects of partial melting and fractionation.

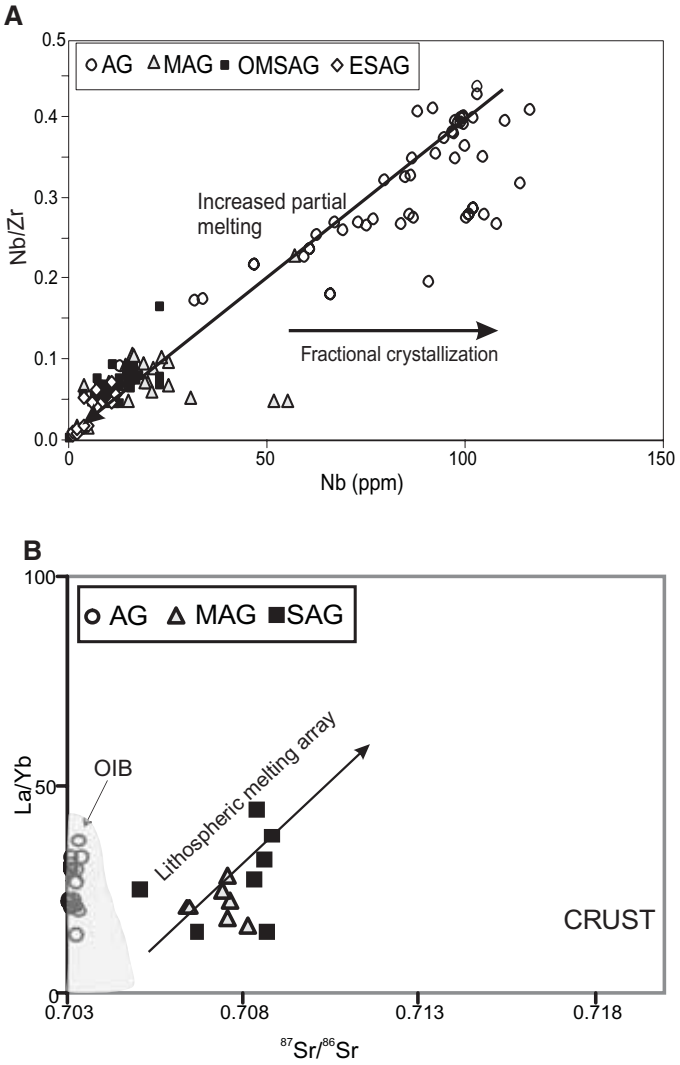

Figure 11. (A) Nb/Zr versus Nb (ppm) diagram for the Eocene subalkaline group (ESAG), Oligocene–early Miocene subalkaline group (OMSAG), mildly alkaline group (MAG), and alkaline group (AG) lavas illustrating the effects of partial melting and fractionation. (B) La/Yb versus $^{87}Sr/^{86}Sr$ diagram for the subalkaline group (SAG), mildly alkaline group (MAG), and alkaline group (AG) lavas illustrating the lithospheric mantle array and ocean island basalt (OIB) field.

(Maury et al., 1992; Schiano et al., 1995). Therefore, it can be deduced that the melt source involved in the genesis of these lavas was a subduction-modified mantle. However, the initiation and establishment of the north-dipping subduction zone at the Hellenic trench postdates much of this phase of the Cenozoic volcanism in the region; hence, these magmas could not have been derived from an active subduction zone at that time. Therefore, the subduction signature inferred from the geochemistry of the calc-alkaline and mildly alkaline groups was possibly inherited from the Late Cretaceous subduction event in the region

(Genç and Yılmaz, 1997; Seyitoğlu et al., 1997; Aldanmaz et al., 2000; Yılmaz et al., 2000). This interpretation implies that the mantle beneath western Anatolia in the Eocene–early Miocene period was heterogeneous and variously enriched by volatiles associated with previous subduction events in the region. The geochemical characteristics outlined earlier might also have been inherited, at least partly, from crustal contamination. The involvement of a melt source containing residual garnet in the formation of the SAG lavas is required to explain their strong HREE depletion (La/Yb up to 50; Fig. 10).

High Pb contents (up to 20 ppm) may also indicate some crustal contamination (Pearce and Peate, 1995). In fact, the $^{87}Sr/^{86}Sr$ (0.709–0.707 for OMSAG, 0.7059 for ESAG) isotope ratios plotted against Rb/Sr (Fig. 12) characterize mantle-derived magmas that appear to have been contaminated by continental crust, as previously suggested (Yılmaz, 1989; Güleç, 1991; Seyitoğlu et al., 1997; Aldanmaz et al., 2000; Yılmaz et al., 2000). However, the Th/Yb (4–24) and Ti/Eu (2280 and 4600) ratios and absolute incompatible-element abundances (e.g., K, Rb, Nb, and Ba) for the least silicic sample of the OMSAG lavas are unlikely to be explained solely by crustal contamination. Therefore, it is clear that both mantle enrichment and crustal contamination are required to explain the evolution of OMSAG magmas.

The large variability of magmatic rock types in the SAG (high-K, medium-K, shoshonitic series, and even ultrapotassic rocks) is likely to have resulted from various geochemical processes, such as heterogeneous source enrichment by an inhomogeneous volatile supply, various rates of melting of the subduction-modified mantle, and various degrees of crustal contamination and differentiation.

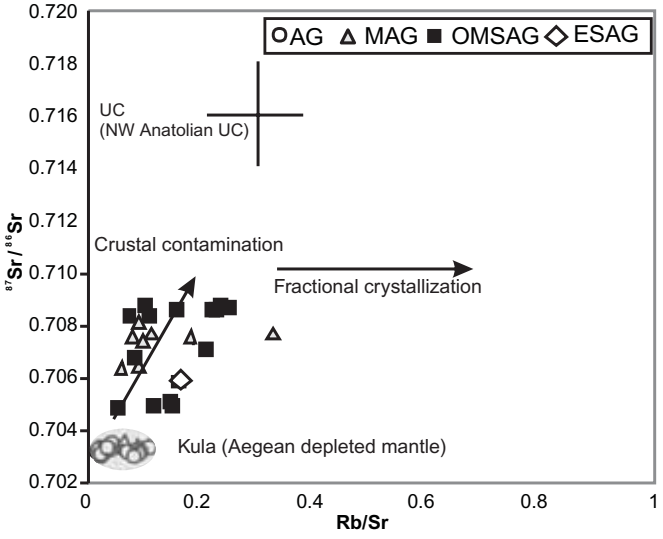

Figure 12. $^{87}Sr/^{86}Sr$ versus Rb/Sr diagram for the Eocene subalkaline group (ESAG), Oligocene–early Miocene subalkaline group (OMSAG), mildly alkaline group (MAG), and alkaline group (AG) lavas illustrating the effects of crustal contamination and fractional crystallization during the evolution of the main volcanic groups in western Anatolia. UC—upper crust.

The high abundances of Sr and the lack of significant Eu anomalies indicate that the melt source in the mantle was plagioclase-free or that plagioclase was not a fractionating phase during melting. The low Nb/La ratios and radiogenic Sr and unradiogenic Nd values indicate that this mantle source was different from a convecting mantle asthenosphere. The $^{87}Sr/^{86}Sr$ ratios are relatively restricted over a range of La/Yb ratios, again suggesting that different degrees of partial melting played a major role in trace-element variability within the SAG (Figs. 10 and 11A and B). The SAG and MAG lavas extend along the projected lithospheric mantle array, whereas the AG lavas plot entirely in the OIB field (Fig. 11B).

As illustrated in the εNd versus $^{87}Sr/^{86}Sr$ diagram (Fig. 9), our three magmatic groups (OMSAG, MAG, and AG) display different isotopic signatures. SAG and MAG lavas exhibit a relatively broad and evolved range of $^{87}Sr/^{86}Sr$ ratios at more restricted εNd values, indicating that the source of SAG lavas must have been enriched and isolated from mantle convection for a long period of time to develop these distinct isotopic values.

The Sr and Nd isotope data; the Ce, Pb, La, and Th contents; and the Nb/Zr ratios of the subalkaline rocks, together with some interelement ratios, collectively suggest that their magmas were derived by different degrees of partial melting of an enriched subcontinental litospheric mantle source (cf. Yılmaz and Polat, 1998) and that these magmas were subsequently contaminated by their interaction with the orogenic crust on their ascent to the surface, acquiring a hybrid character.

Lavas of the OMSAG are strongly enriched in LILE and LREE compared to those of the ESAG and island-arc basalts (Fig. 6). These chemical features suggest either a greater subduction component in the melt source region of these lavas or a greater extent of crustal assimilation during the evolution of their magmas. The lower Pb contents and Th/Yb ratios (1–17 ppm and 3.84, respectively) of the ESAG and the higher Pb contents and Th/Yb ratios (12.2–20 ppm and 5–24, respectively) of the OMSAG lavas indicate higher degrees of crustal contamination of the OMSAG magmas in comparison to the ESAG lavas.

The Sr and Nd isotopic ratios of the OMSAG lavas reflect high degrees of crustal contamination. The SAG lavas, which erupted during the Eocene and the early–middle Miocene, have decreasing Sr isotope initial ratios at approximately constant $^{143}Nd/^{144}Nd$ isotopic compositions (0.5123–0.5127; Fig. 13). The ESAG and OMSAG lavas plot in a field between the MORB and crustal (Aegean sea sediments and Aegean granitoids) fields, indicating a hybrid composition (Fig. 13). We do not have enough isotope data from the ESAG lavas (only one sample), but the Nd and Sr isotope values of the OMSAG lavas have significantly higher $^{87}Sr/^{86}Sr$ (0.707–0.7087) and lower $^{143}Nd/^{144}Nd$ (0.5122–0.5127) initial ratios, suggesting increasing degrees of crustal contamination or assimilation and fractional

crystallization and a decreasing amount of subduction signature from the late Eocene to the early Miocene; these conclusions may also be supported by the $^{87}Sr/^{86}Sr$ versus age relationships shown in Figure 14. The subalkaline magmatism was predominant between 37 and 16 Ma. There is an increase in the $^{87}Sr/^{86}Sr$ ratio from 37 Ma to 22 Ma in this diagram, although the lack of data from the interval of 26–22 Ma makes it difficult to evaluate the degree of crustal contamination during this period. It is obvious that the $^{87}Sr/^{86}Sr$ ratios of the Eocene and Oligocene lavas are significantly lower than those of the early Miocene (ca. 22–16 Ma) lavas. These different Sr isotope values can be explained either by different melt sources for the lavas aged 37–26 Ma (Eocene and Oligocene) and those aged 22–16 Ma (early to middle Miocene) or by increasing amounts of crustal contamination from 37 to 22 Ma. However, our observation that the Oligocene lavas display similar geological and geochemical features to those of the early to middle Miocene lavas suggests their generation from a common melt source. Therefore, increasing amounts of crustal contamination are likely to have caused these different isotopic compositions. When we evaluate the geological information together with our limited isotopic data and interelement ratios, we can deduce that the stronger enrichment in LILE and LREE of OMSAG may indicate increasing amounts of crustal contamination and a decreasing subduction signature rather than a greater subduction component in the source region.

Mildly Alkaline Group

Major- and trace-element characteristics, interelement ratios, and isotope systematics indicate that the MAG lavas were derived from slightly to moderately evolved magmas and that they show transitional geochemical characteristics between the SAG and AG rocks. In the Al_2O_3 versus MgO diagram (Fig. 5), they display a broad negative correlation, suggesting that despite the presence of plagioclase phenocrysts in more evolved samples, plagioclase fractionation was not a significant petrogenetic process. Ni (up to 250 ppm) and MgO (up to 10 wt%) in the most primitive MAG samples are high relative to the ESAG and OMSAG lavas and display positive trends consistent with a melting curve indicating olivine and clinopyroxene fractionation (Fig. 5) during their evolution (Hart and Davis, 1978). The lack of plagioclase fractionation is further supported by the lack of negative Eu anomalies and the consistently high Sr contents of the rocks (Fig. 5).

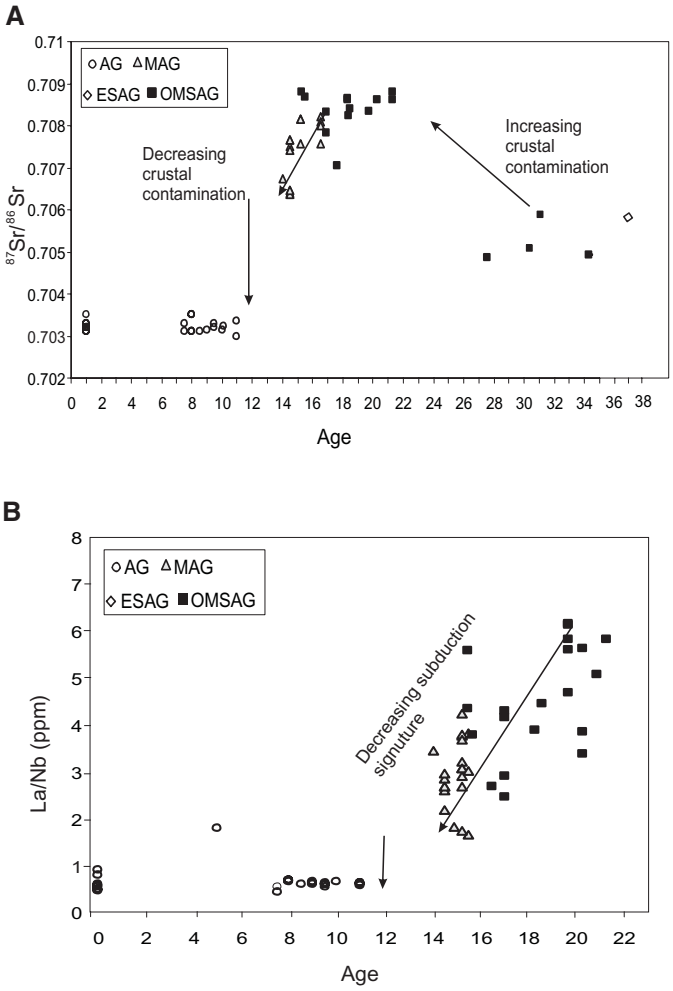

Figure 14. (A) $^{87}Sr/^{86}Sr$ versus age diagram for the Eocene subalkaline group (ESAG), Oligocene–early Miocene subalkaline group (OMSAG), mildly alkaline group (MAG), and alkaline group (AG) lavas. (B) La/Nb (ppm) versus age (Ma) diagram for the ESAG, OMSAG, MAG, and AG lavas.

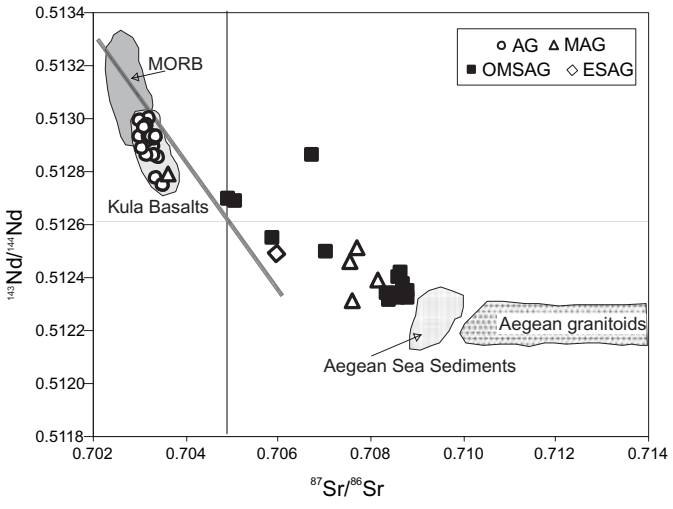

Figure 13. $^{143}Nd/^{144}Nd$ versus $^{87}Sr/^{86}Sr$ diagram for the Eocene subalkaline group (ESAG), Oligocene–early Miocene subalkaline group (OMSAG), mildly alkaline group (MAG), and alkaline group (AG) lavas. MORB—mid-ocean ridge basalt.

Intermediate to felsic products of the MAG show MORB-normalized multielement patterns (e.g., enrichment in Rb, Th, and K and negative anomalies in Ba, Sr, P, and Ti), suggesting their possible derivation from basaltic magmas through crystal fractionation (Fig. 6). The trace-element patterns of this group are consistent with the derivation of their magmas from an incompatible-element-enriched source, as evidenced by negative Ta and Nb anomalies, enriched LREE, and low Rb/Sr ratios. These features of the MAG lavas are similar to those of rocks that form at convergent margin settings rather than to alkali basalts that form within plate or other continental extensional settings.

MORB-normalized trace-element patterns and chondrite-normalized REE patterns also indicate that there are some similarities between the SAG and MAG rocks, as discussed in the previous section. Both the SAG and MAG basalts are enriched in LILE, LREE, and HFSE relative to MORB, and both have high LILE/HFSE ratios (e.g., Ba/Nb). Based on these lines of evidence, we deduce that melting of a subduction-modified lithospheric mantle was still involved in the evolution of MAG magmas. However, the MAG lavas have significantly lower La /Nb (1.7–4), Zr/ Nb (9–15; Fig. 8), and $^{87}Sr/^{86}Sr$ (0.704–0.7077) ratios (Fig. 9) and higher $^{143}Nd/^{144}Nd$ (0.5124–0.5127; Fig. 12) ratios in comparison to the SAG lavas; hence, they display intermediate values between the SAG and AG lavas. Their $(La/Yb)_n$ ratios are lower than those of the SAG lavas, ranging between 9 and 17 (Fig. 7), which is transitional between asthenospheric and lithospheric mantle melts. These features indicate that both lithospheric and asthenospheric mantle components contributed to the MAG source region.

The available petrological and geochemical data collectively indicate that, in general, the MAG lavas have transitional compositions and that they form a petrogenetic and temporal link between the SAG and AG lavas. Figure 14 shows the late Cenozoic magmatic evolution of western Anatolia over time. It appears that the mildly alkaline lavas started at ca. 16 Ma, close to the end of the subalkaline magmatism. The $^{87}Sr/^{86}Sr$ ratio decreases from subalkaline to mildly alkaline to strongly alkaline-type magmatism through time. This decrease is less pronounced passing from subalkaline to mildly alkaline magmatism, but makes a rather sharp jump from mildly alkaline to alkaline magmatism. The La/Nb versus age diagram in Figure 14B also shows similar temporal relationships in the La/Nb ratio over time. The compositional shift to lower $^{87}Sr/^{86}Sr$, lower La/Nb and Zr/Nb (Fig. 8B), and higher Nb/Sr, Nb/Ba, and $^{143}Nd/^{144}Nd$ indicates the influence of incoming asthenospheric melts.

The observed relationships between La/Nb and age, εNd and $^{87}Sr/^{86}Sr$, and Zr/Nb and La/Nb (Figs. 8B, 9, and 14A and B) show that there is an apparent decrease in the La/Nb, Zr/Nb, and $^{87}Sr/^{86}Sr$ ratios from the SAG to the AG lavas. This decrease is less pronounced passing from the SAG to the MAG lavas but rather sharp from the MAG to the AG lavas. Gradual passing from the SAG to the MAG lavas followed by a sharp jump to the AG lavas (Figs. 8B, 9, and 14) was likely caused by the melting of a subduction-modified lithospheric mantle and its subsequent modification by percolating asthenospheric magmas or related fluids that further affected the compositions of subsequent liquids produced by partial melting. As a result, the subduction-related geochemical signature of the SAG was diminished, whereas the MAG acquired lower La/Nb, Zr/Nb, and $^{87}Sr/^{86}Sr$ ratios and higher $^{143}Nd/^{144}Nd$ ratios with time.

Alkaline Group

The AG is represented by strongly alkaline lavas displaying sodic alkaline features. The K_2O/Na_2O ratios range between 0.3 and 0.7, and the Mg #s are highly variable (51–70), with some samples having nearly primitive values (Mg # ~70–73). Some alkaline rocks appear to be differentiated, as evidenced by their low Mg # (<60) and Ni and Cr contents. The MgO covariation diagrams, especially the Ni-MgO and Al_2O_3-MgO covariations, presumably reflect the olivine and clinoproxene fractionation crystallization (Fig. 5).

The AG lavas are characterized by low $^{87}Sr/^{86}Sr$ (0.70302–0.70349) and high $^{143}Nd/^{144}Nd$ (0.51277–0.51294) ratios and have OIB-like trace-element patterns characterized by enrichment in both LILE and HFSE (Fig. 6). They plot in the OIB field in the La/Yb versus $^{87}Sr/^{86}Sr$ diagram, indicating an OIB-like asthenospheric component in their melt source. However, the enrichment levels of HFSE (Nb and Ta) and some trace-element ratios, such as those for Rb/Nb and K/Nb, are higher than those of typical OIB; this indicates melt contribution(s) from a lithospheric mantle source. Based on their high LILE abundances and high MREE/HREE ratios, Aldanmaz et al. (2000) and Alıcı et al. (2002) suggested that the AG lavas were generated from a garnet-bearing lherzolitic mantle source.

SPATIAL AND TEMPORAL RELATIONS BETWEEN TECTONICS AND MAGMATISM: GEODYNAMIC MODEL

Collision Tectonics, Slab Break-Off, and Crustal Thickening

Emplacement of the Cretaceous ophiolites onto the Tauride platform along the Izmir-Ankara-Erzincan suture zone and partial subduction of the platform edge that led to its high-*P,* low-*T* metamorphism (Sherlock et al., 1999; Okay, 2002; Ring and Layer, 2003; Ring et al., 2003) in the Late Cretaceous mark the initial stages of collision tectonics in western Anatolia (Figs. 15 and 16). The terminal closure of the Neo-Tethyan seaway resulted in the collision of the Sakarya continent with the Tauride platform during the Eocene, which in turn caused regional deformation, metamorphism, and crustal thickening. This Barrovian-type, collision-driven regional metamorphism was responsible for the development of high-grade rocks in the Kazdag and Menderes metamorphic massifs. Resistance of the buoyant Tauride platform crust to subduction and its arrest

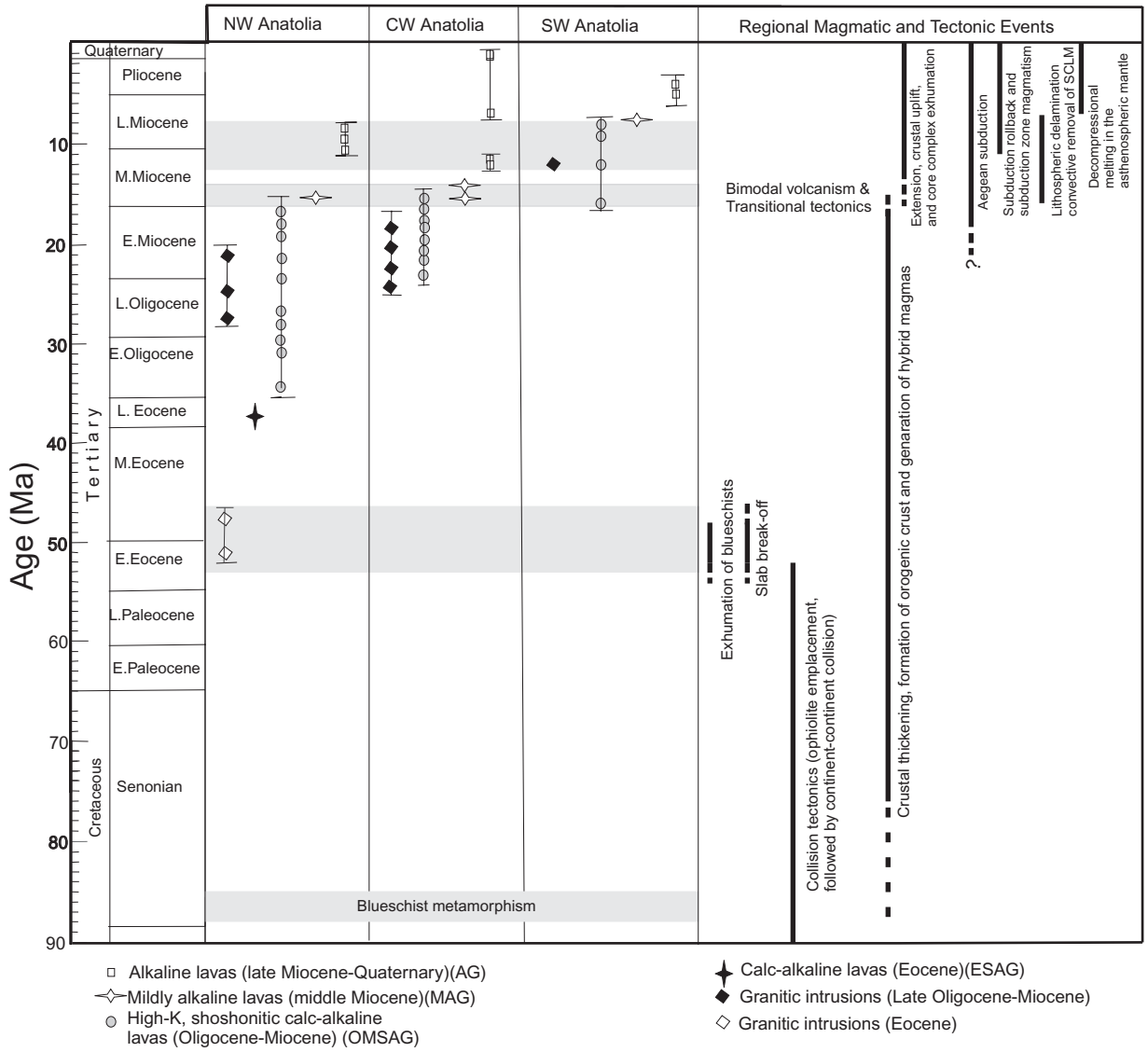

Figure 15. Spatial and temporal relations between major postcollisional tectonic events and magmatic episodes during the late Mesozoic and Cenozoic evolution of western Anatolia. See text for discussion. SCLM—subcontinental lithospheric mantle. The geological timescale used is from Harland et al. (1989).

of the north-dipping subduction zone resulted in isostatic uplift of its partially subducted passive margin, exhumation of high-*P* rocks, and rapid denudation of upper-crustal rocks, leading to widespread flysch formation during the early to the middle Eocene (Ring et al., 2003, and references therein).

With continued continental collision, the leading edge of the subducted Neo-Tethyan slab possibly broke off from the rest of the continental lithosphere, resulting in the development of an asthenospheric window (Fig. 16). Slab detachment and break-off is a natural response to the gravitational settling of subducted lithosphere in continental collision zones as a result of a decrease in the subduction rate caused by the positive buoyancy of partially subducted continental lithosphere (Davies and von Blanckenburg, 1995; Wortel and Spakman, 2000; Gerya et al., 2004; Seghedi et al., 2004). As the downgoing oceanic plate breaks off, the asthenosphere rises rapidly and juxtaposes itself against the thickened mantle lithosphere in the collision zone (Fig. 16, ca. 54–48 Ma). The heating up of this overriding lithosphere by conduction results in melting of the metasomatized and hydrated layers, producing potassic, calc-alkaline magmas. Crustal melting at shallow depths that is induced by asthenospheric upwelling causes granitic or rhyolitic magmatism. Middle to late Eocene emplacement of widespread granitoid plutons in northwestern Anatolia, mainly through the

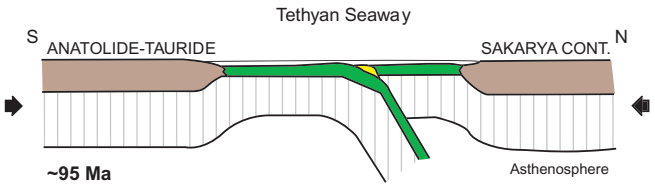

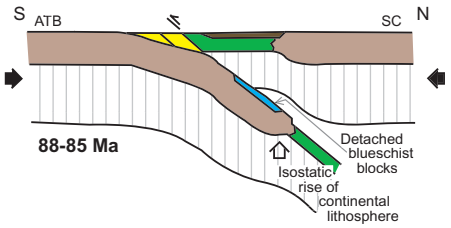

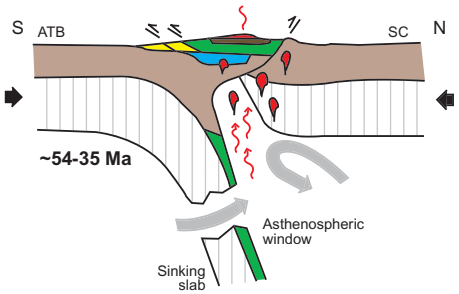

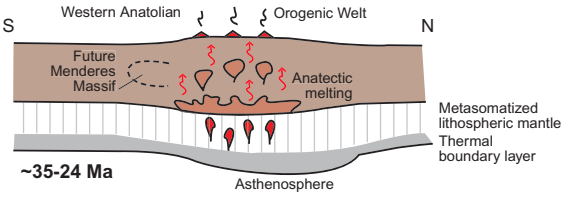

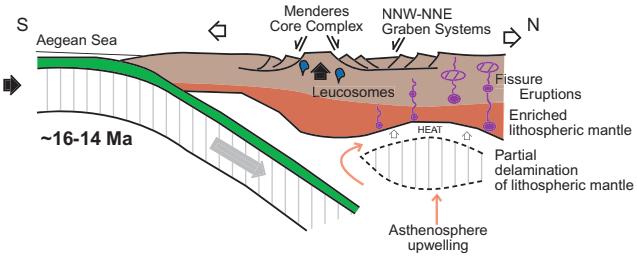

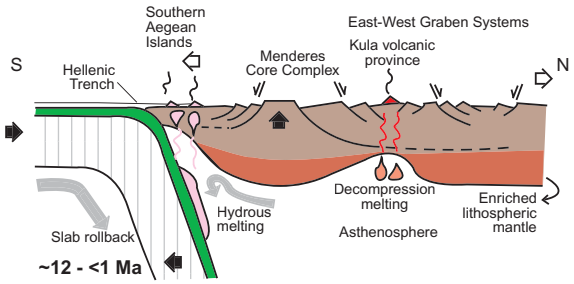

Symbols:

- Regional extension
- Regional compression
- SAG magmas
- Fractional crystallization
- MAG magmas
- AG magmas
- Subduction-related magmas
- Oceanic crust
- Continental crust
- Blueschist rocks
- Subduction-accretion
- Sedimentary basin

GEODYNAMICS	MELT SOURCE AND MAGMATIC PRODUCTION
Intraoceanic subduction within Neo-Tethys; closure of IAE Ocean due to ATB-Sakarya Continent convergence.	Supra subduction zone and active margin magmatism along the Sakarya Continent.
ATB-trench collision, ophiolite emplacement, and partial subduction of ATB passive margin; high-*P* metamorphism of passive margin rocks; isostatic rebound of continental lithosphere in downgoing plate.	Onset of postcollisional magmatism.
Continent-continent collision; slab break-off and asthenospheric window development.	Metasomatized lithospheric mantle source. Medium-K calcalkaline magmatism, producing plutons and felsic to basic volcanic rocks. Assimilation and fractional crystallization.
Development of an orogenic welt with thick crust and high surface elevation; subsequent orogenic collapse (post-24 Ma).	Anatectic melting of overthickened orogenic crust. Metasomatized lithospheric mantle-derived plus crustal melts, producing high-K shoshonitic magmas; plutonism and felsic to basic volcanism (hybrid in nature).
Onset of Aegean subduction at Hellenic trench; crustal-scale extension, core complex formation, and structural graben development.	Upwelling of the hot asthenosphere below thinned continental lithosphere mantle; lithospheric mantle and asthenospheric mantle and limited lithospheric mantle-derived melts, slightly contaminated by continental crust. Medium-alkaline and calc-alkaline magmatism, bimodal volcanism.
Steepening of Aegean subduction zone; southwest retreat of Hellenic trench; SW escape of Anatolian plate and N-S, lithospheric-scale extension in west Anatolia; E-W graben development.	Enriched asthenospheric mantle-derived melt. Alkaline volcanism. Decompression melting of asthenospheric mantle; OIB-type volcanism (uncontaminated) near major fault systems and/or fault intersections. Subduction-related volcanism on south Aegean islands (Milos, Santorini, Methana).

Decreasing subduction signature
Increasing crustal contamination

Decreasing subduction signature
Decreasing crustal contamination

Izmir-Ankara-Erzincan suture zone and the Sakarya continent (Orhaneli, Topuk, Göynükbelen, etc.), was a direct result of heat flux through this window and associated thermal perturbation that caused melting of the metasomatized continental lithospheric mantle. Similar models have been put forward to explain the spatial and temporal relations between slab detachment processes and magmatism in Anatolia and other orogenic belts (Davies and von Blanckenburg, 1995; Aite and Gélard, 1997; De Boorder et al., 1998; Maury et al., 2000; Coulon et al., 2002; Keskin, 2003; Şengör et al, 2003; Köprübasi and Aldanmaz, 2004). Major- and trace-element compositions of I-type granitoid rocks (54–35 Ma) in northwestern Anatolia indicate their origin by melting of a subduction-modified mantle source that had been enriched in mobile incompatible elements (Altunkaynak, 2004; Köprübasi and Aldanmaz, 2004), and this interpretation is consistent with postcollisional magmatism driven by slab break-off in other orogenic belts (Schliestedt et al., 1987; Hansmann and Oberli, 1991; Davies and von Blanckenburg, 1995; Nemcok et al., 1998).

The majority of the ESAG lavas have basaltic and basaltic andesite compositions, and the major- and trace-element characteristics of the more evolved members of this group indicate olivine and clinopyroxene fractionation from mafic (basaltic) magmas. Geochemical and petrological characteristics of this group suggest that the melt source region of its magmas was the subcontinental lithospheric mantle modified by previous subduction event(s). Trace-element variations and interelement ratios collectively suggest that the magmas of the ESAG show similar patterns to those of subduction-related arc magmas (Fig. 6; Pearce, 1982; Thorpe et al., 1982; Cox and Hawkesworth, 1985; Pearce et al., 1990; Davidson et al., 1991; Walker et al., 1991; Pearce and Peate, 1995; Genç and Yılmaz, 1997). This subduction signature gradually decreases in other groups (OMSAG and MAG) from the late Eocene to the early middle Miocene.

Continued crustal deformation in the collision zone, cessation of subduction, and replacement of the cold oceanic lithosphere by asthenosphere collectively led to the development of thick continental crust and rapid uplift of the orogen, which in turn created an "orogenic welt" with high surface elevation by the latest Eocene–Oligocene (ca. 35–24 Ma; Figs. 15 and 16). Regional tectonic models (McKenzie, 1972; Şengör et al., 1984; Seyitoğlu and Scott, 1996; Dilek and Whitney, 2000) suggest that the continental crust in western Anatolia was in excess of 50 km in thickness by the late Eocene as a result of continued north-south compression. Anatectic melting of this overthickened orogenic crust generated leucogranitic intrusions (Dora et al., 1987; Yılmaz, 1990). Metasomatized lithospheric mantle-derived melts and crustal melts produced high-K shoshonitic magmas that formed suites of plutonic, hypabyssal, and volcanic rocks of felsic to basic compositions (hybrid in nature) throughout northwestern and central–west Anatolia during the Oligo-Miocene (Bingöl et al., 1994; Altunkaynak and Yılmaz, 1998; Genç, 1998; Karacik and Yılmaz, 1998). Examples of major igneous complexes of this magmatic episode include, from west to east, the Kestanbol, Kozak, Ilica, Çataldag, and Bayramiç plutons (Fig. 2). This Oligo-Miocene igneous phase with widespread plutonism and bimodal volcanism in northwestern and central–western Anatolia marks the last episode of magmatism before the onset of regional tectonic extension and the collapse of the west Anatolian orogenic welt (Yılmaz, 1990; Seyitoğlu et al., 1997; Altunkaynak and Yılmaz, 1998).

Orogenic Collapse, Lithospheric Delamination, and Extensional Magmatism

Western Anatolia and the adjacent Aegean region underwent regional extensional deformation in the Miocene and onward, resulting in crustal-scale tectonic denudation and exhumation of high-grade metamorphic rocks (Meulenkamp et al., 1988; Jolivet et al., 1994a; Lister and Forster, 1996; Ring et al., 2003). Recent studies have shown that unroofing of the Kazdag and Menderes metamorphic core complexes and the emplacement of synextensional intrusions may have occurred as early as in the latest Oligocene and the early Miocene (Bozkurt and Satir, 2000; Okay and Satir, 2002; Ring and Collins, 2005). NNW- and NNE-trending graben systems and basins that were developed during the early to the middle Miocene became the major depocenters for clastic material derived from erosional unloading of the core complexes. These graben systems contain lava flows, pyroclastic rocks, and lahar deposits ranging in age from 18 to 14 Ma (Seyitoğlu and Scott, 1991; Seyitoğlu et al., 1997; Inci, 1998; Yılmaz et al., 2000, 2001; Bozkurt, 2003), indicating that extensional faulting and deposition were attended by volcanism.

Crustal thinning due to regional extensional tectonics played an important role in the petrogenesis and chemical evolution of magmatism in western Anatolia starting in the middle Miocene. Magmas of the MAG derived from the subcontinental lithospheric mantle (SCLM) and/or the lithosphere-asthenosphere boundary were transported to the surface along transtensional fault systems, with little or no interaction with the crust. Both calc-alkaline and mildly alkaline lavas (dominant) were erupted during this transitional regime around 16–14 Ma (Altunkaynak et al., 2004), giving the western Anatolian volcanism a bimodal character (Fig. 16). Petrogenetic modeling of these volcanic rocks suggests that their magmas were derived mainly from asthenospheric mantle with limited input from the lithospheric mantle-derived melts that evolved through assimilation and fractional crystallization (Güleç, 1991; Seyitoğlu et al., 1997; Aldanmaz et al., 2000; Yılmaz et al., 2001; Altunkaynak et al.,

Figure 16. Sequential tectonic diagram depicting the late Mesozoic–Cenozoic geodynamic evolution of western Anatolia. AG—alkaline group, MAG—mildly alkaline group, and SAG—subalkaline group magmas; ATB—Anatolide-Tauride block; IAE—Izmir-Ankara-Erzincan; OIB—ocean island basalt. See the text for discussion.

2004). However, the effects of assimilation and crustal contamination appear to have decreased through time, as indicated by the increased production of basaltic rocks from the early to the middle Miocene.

The formation and petrogenesis of the MAG lavas in western Anatolia during 16–14 Ma may be best explained by lithospheric delamination and/or partial convective removal of the SCLM (Fig. 16). In the case of lithospheric delamination, the entire SCLM is peeled off (Bird, 1979; Aldanmaz et al., 2000; Williams et al., 2004), whereas in partial removal of the SCLM by convective thinning only the lower part of the SCLM is removed (Houseman et al., 1981; England and Houseman, 1989; Lenardic and Kaula, 1995; Turner et al., 1996; Williams et al., 2004). The replacement of the entire SCLM or its lower part by the hot asthenosphere provides the necessary heat source (and basaltic melts produced by decompressional melting of the asthenosphere in the case of lithospheric delamination), which in turn results in partial melting of metasomatized regions in the mantle. We envision that this enriched mantle-derived melt produced mildly alkaline to alkaline lavas in western Anatolia (Figs. 15 and 16). We interpret the inferred crustal uplift, tectonic extension, and continued core complex exhumation in western Anatolia during 16–14 Ma to have been mainly coeval with mildly alkaline magmatism as a result of thermal relaxation and dissipation of the potential energy excess via normal faulting in the aftermath of delamination and/or partial removal of the SCLM. The delamination model may also explain the apparent southward migration of the MAG volcanism during the middle to the late Miocene (Fig. 15).

Initiation of the Hellenic Subduction, Asthenospheric Upwelling, and Alkaline Magmatism

The initiation of subduction along the Hellenic trench is inferred to have occurred ca. 13 Ma (LePichon and Angelier, 1979), although some researchers think that it might have started as early as 26 Ma (Meulenkamp et al., 1988). The Hellenic subduction was most likely established by the middle Miocene, placing western Anatolia in a back-arc tectonic setting (Pe-Piper and Piper, 1989, this volume; Jolivet et al., 1994b; Mc Clusky et al., 2000; Ring and Layer, 2003).

The late Miocene–Pliocene alkaline volcanism (ca. 5–<1 Ma; Figs. 15 and 16) has OIB-type trace-element patterns whose geochemical characteristics suggest enriched asthenosphere as the magma source of the late Miocene alkaline volcanism. The apparent lack of negative Ta or Nb anomalies in the trace-element patterns of these alkaline basalts indicates that their magmas were not affected by subduction-generated fluids or by crustal contamination. However, volcanic rocks on the south Aegean arc farther south near the Hellenic trench show typical calc-alkaline characteristics (1–3 wt% K_2O; enrichment in LILE; low Nb, Ta, and Ti; and hydrous phenocrysts), suggesting that their magmas were derived from hydrous melting in the asthenopsheric wedge above the north-dipping Aegean subduction zone (Fig. 16; Pe-Piper and Piper, this volume). It is inferred that the slab roll-back associated with this subduction zone has been the major driving force for extension in the arc-forearc region since 12–11 Ma (Meulenkamp et al., 1988; Jolivet et al., 1994a; Dilek, this volume).

Trace-element and isotopic compositions of the final products of western Anatolian magmatism are consistent with derivation of their magmas from both asthenospheric and lithospheric mantle sources. Contribution of lithospheric mantle to asthenosphere-derived melts could be responsible for their enrichment in incompatible elements relative to the OIB. Assimilation and fractional crystallization modeling of the AG lavas, as in the Kula volcanic rocks (Fig. 16), indicate that crustal contamination was not an important process in their evolution, whereas fractional crystallization played an important role in their development (Aldanmaz et al., 2000; Alıcı et al., 2002). This group represents the last products of magmatism in western Anatolia related to the late Miocene–Pliocene extensional regime that was driven by lithospheric thinning, asthenospheric upwelling, and decompressional melting of this asthenospheric mantle. Major eruptive centers of this latest volcanic phase appear to be situated near significant fault systems or at the intersections of major lithospheric-scale fault systems (such as in Kula), which may have acted as natural conduits for magma transport. This fault-controlled eruption of the latest-stage AG lavas may explain the lack of crustal contamination in their evolution.

CONCLUSIONS

Postcollisional volcanism in western Anatolia followed the collision of the Sakarya and Tauride continental blocks in the early Eocene and occurred in discrete pulses through time. The nature and spatial and temporal distribution of this volcanism were affected by changes in mantle dynamics, regional tectonics and crustal evolution, and geodynamic events in the eastern Mediterranean region throughout the Cenozoic. We identify three main episodes of postcollisional volcanism, with different geochemical characteristics, that appear to have propagated from north to south through time in western Anatolia.

The first episode of volcanism evolved during the Eocene and the Oligo-Miocene and was subalkaline in nature, producing medium- to high-K calc-alkaline and shoshonitic rocks. Partial melting of subduction-enriched subcontinental lithospheric mantle and assimilation and fractional crystallization were important processes for the genesis and evolution of their parent magmas, which experienced decreasing subduction influence and increasing crustal contamination through time. Accompanied by extensive plutonism, particularly in the north, the subalkaline volcanism in western Anatolia overlapped with continued regional compression and the development of a thick orogenic crust and was influenced by an influx of asthenospheric heat and melts provided by slab break-off.

The second main episode of postcollisional volcanism in

western Anatolia occurred during 16–14 Ma, marking a transitional period in both the tectonic and the magmatic evolution of the region. Extensional tectonics had replaced the regional compression by the middle Miocene, following the initial collapse of the western Anatolian orogenic welt, and had resulted in the development of metamorphic core complexes and horst-graben structures. Volcanism accompanying this regional extension produced mildly alkaline rocks that show a decreasing amount of crustal contamination and decreasing subduction influence through time. Although melting of a subduction-modified lithospheric mantle continued during this transitional period of volcanism, asthenospheric mantle-derived melt contributions played a major role in the generation of the MAG magmas. We infer that this asthenospheric melt contribution was a result of lithospheric delamination and/or partial convective removal of the subcontinental lithospheric mantle. The initiation of the Hellenic subduction beneath the Aegean extensional province was also in progress during this time.

The third episode of volcanism in western Anatolia started ca. 12 Ma, following a short time gap after the transitional episode of magmatism, and continued until prehistoric times. The trace-element and isotopic signatures of volcanic rocks (basalts, basanites, and tephrites) produced during this phase indicate that the source region of this alkaline magmatism carried no subduction component and that the alkaline magmas were not affected by crustal contamination processes. The main source of alkaline volcanism was decompressional melting of the asthenospheric mantle flowing beneath the significantly attenuated continental lithosphere in the Aegean extensional province. Lithospheric-scale extensional fault systems and their intersections provided natural conduits for the transport of uncontaminated alkaline magmas to the surface in discrete locations. The southwestward retreat of the Hellenic trench and associated subduction roll-back have resulted in arc volcanism and crustal extension in the southern Aegean throughout the latest Miocene and the Quaternary.

ACKNOWLEDGMENTS

This study has been supported by a grant from TUBITAK (CAYDAG-101Y006) to ŞA and by Committee of Faculty Research and Hampton funds from Miami University to YD. Discussions with Erdin Bozkurt, Ş. Can Genç, Cahit Helvaci, Eric Sandvol, Yılmaz Savaşçin, and Yücel Yılmaz on various aspects of the Cenozoic geology and geodynamics of western Anatolia have been most helpful to us in developing the ideas and interpretations presented in this article. Thorough reviews by Kendall Hauer, Ali Polat, and Paul T. Robinson helped us improve the paper.

REFERENCES CITED

Aite, M.O., and Gélard, J.P., 1997, Distension néogène post collisionnelle sur le transect de Grande Kabylie (Algeria): Bulletin de la Société Géologique de France, v. 168, no. 4, p. 423–436.

Akay, E., and Erdogan, B., 2004, Evolution of Neogene calc-alkaline to alkaline volcanism in the Aliaga-Foca region (Western Anatolia, Turkey): Journal of Asian Earth Science, v. 24, p. 367–387, doi: 10.1016/j.jseaes.2004.01.015.

Aldanmaz, E., Pearce, J., Thriwall, M.F., and Mitchell, J., 2000, Petrogenetic evolution of late Cenozoic, post-collision volcanism in western Anatolia, Turkey: Journal of Volcanology and Geothermal Research, v. 102, p. 67–95, doi: 10.1016/S0377-0273(00)00182-7.

Alıcı, P., Temel, A., and Gourgaud, A., 2002, Pb-Nd-Sr isotope and trace element geochemistry of Quaternary extension-related alkaline volcanism: A case study of Kula region (western Anatolia, Turkey): Journal of Volcanology and Geothermal Research, v. 115, p. 487–510, doi: 10.1016/S0377-0273(01)00328-6.

Altunkaynak, Ş., 1996, Geologic and petrologic investigation of the relationship of young volcanism and plutonism in the area located between Bergama and Ayvalik [Ph.D. thesis]: Technical University of Istanbul, Institute of Science, Turkey, 402 p. (in Turkish with an extended abstract in English).

Altunkaynak, Ş., 2004, Post collisional multistage magmatism in northwest Anatolia (Turkey): Geochemical and isotopic study of Orhaneli magmatic associations, *in* 32nd International Geological Congress, Florence, Italy, August 20–28, Abstracts (Part 2), p. 1298.

Altunkaynak, Ş., and Yılmaz, Y., 1998, The mount Kozak magmatic complex, Western Anatolia: Journal of Volcanology and Geothermal Research, v. 85, p. 211–231, doi: 10.1016/S0377-0273(98)00056-0.

Altunkaynak, Ş., and Yılmaz, Y., 1999, The Kozak Pluton and its emplacement: Geological Journal, v. 34, p. 257–274, doi: 10.1002/(SICI)1099-1034(199907/09)34:3<257::AID-GJ826>3.0.CO;2-Q.

Altunkaynak, Ş., Rogers, N., and Kelley, S., 2004, Petrogenetic evolution of the bimodal Cenozoic volcanism in western Anatolia (Turkey): The Foça volcanic center, *in* 32nd International Geological Congress, Florence, Italy, August 20–28, Abstracts (Part 2), p. 1294–1295.

Barka, A., and Reilinger, R., 1997, Active tectonics of the Eastern Mediterranean region: Deduced from GPS, neotectonic and seismicity data: Annali Di Geofisica, v. 40, p. 587–610.

Bingöl, E., Delaloye, M., and Ataman, G., 1982, Granitic intrusions in Western Anatolia: A contribution of the geodynamic study of this area: Eclogae Geologicae Helvetiae, v. 75, p. 437–446.

Bingöl, E., Delaloye, M., and Genç, S., 1994, Magmatism of northwestern Anatolia, *in* International Volcanological Congress, IAVCEI 1994, Excursion Guide (A3), 56 p.

Bird, P., 1979, Continental delamination and the Colorado Plateau: Journal of Geophysical Research, v. 84, p. 7561–7571.

Borsi, S., Ferrara, G., Innocenti, F., and Mazzuoli, R., 1972, Geochronology and petrology of recent volcanics in the eastern Aegean Sea (West Anatolia and Lesbos island): Bulletin of Volcanology, v. 36, p. 473–496.

Boynton, W.V., 1984, Geochemistry of the rare-earth elements: Meteorite studies, *in* Henderson, P., ed., Rare earth element Geochemistry: Amsterdam, Elsevier, p. 63–114.

Bozkurt, E., 2001, Neotectonics of Turkey: A synthesis: Geodinamica Acta, v. 14, p. 3–30, doi: 10.1016/S0985-3111(01)01066-X.

Bozkurt, E., 2003, Origin of NE-trending basins in western Turkey: Geodinamica Acta, v. 16, p. 61–81, doi: 10.1016/S0985-3111(03)00002-0.

Bozkurt, E., and Park, R.G., 1997, Microstructures of deformed grains in the augen gneisses of southern Meneders Massif and their tectonic significance: Geologische Rundschau, v. 86, p. 103–119, doi: 10.1007/s005310050125.

Bozkurt, E., and Satir, M., 2000, The southern Menderes Massif (western Turkey): Geochronology and exhumation history: Geological Journal, v. 35, p. 285–296, doi: 10.1002/gj.849.

Catlos, E.J., Çemen, I., Isik, V., and Seyitoğlu, G., 2002, In situ timing constraints from the Menderes massif, western Turkey: Geological Society of America Abstracts with Programs, v. 34, no. 6, p. 180.

Çemen, I., Seyitoğlu, G., and Isik, V., 2002, Extensional tectonics in southern Basins and Ranges, USA and in western Turkey: A review of similarities, differences, and problems: Geological Society of America Abstracts with Programs, v. 34, no. 6, p. 177.

Coulon, C., Megartsi, M., Fourcade, S., Maur, R.C., Bellon, H., Hacini, A.L., Cotten, J., Coutelle, A., and Hermitte, D., 2002, Post collisional transition from calc-alkaline to alkaline volcanism during the Neogene in Oranie (Algeria): Magmatic expression of a slab breakoff: Lithos, v. 62, p. 87–110, doi: 10.1016/S0024-4937(02)00109-3.

Cox, K.G., and Hawkesworth, C.J., 1985, Geochemical stratigraphy of the Deccan Traps at Mahabalaeshwar, Western Ghats, India: Its implications for open system magmatic processes: Journal of Petrology, v. 26, p. 355–377.

Davidson, J.P., Harmon, R.S., and Worner, G., 1991, The source of central Andean magmas: Some considerations, *in* Harmon, R.S., and Rapela, C.W., eds., Andean magmatism and its tectonic setting: Geological Society of America Special Paper 265, p. 233–243.

Davies, J.H., and von Blanckenburg, F., 1995, Slab breakoff: A model of lithosphere detachment and its test in the magmatism and deformation of collisional orogens: Earth and Planetary Science Letters, v. 129, p. 85–102, doi: 10.1016/0012-821X(94)00237-S.

De Boorder, H., Spakman, W., White, S.H., and Wortel, M.J.R., 1998, Late Cenozoic mineralization, orogenic collapse and slab detachment in the European Alpine Belt: Earth and Planetary Science Letters, v. 164, p. 569–575, doi: 10.1016/S0012-821X(98)00247-7.

Demirtasli, E., Turhan, N., Bilgin, A.Z., and Selim, M., 1984, Geology of the Bolkar Mountains, *in* Tekeli, O., and Göncüoglu, M.C., eds., Geology of the Taurus Belt: Proceedings of the International Symposium, Geology of the Taurus Belt, Mineral Research & Exploration Institute of Turkey (MTA), Ankara, p. 125–141.

Dewey, J.F., Hempton, M.R., Kidd, W.S.F., Saroğlu, F., and Şengör, A.M.C., 1986, Shortening of continental lithosphere: The neotectonics of Eastern Anatolia—A young collision zone, *in* Coward, M.P., and Ries, A.C., eds., Collision zone tectonics: Geological Society of London Special Publication 19, p. 3–36.

Dilek, Y., and Moores, E.M., 1990, Regional tectonics of the Eastern Mediterranean ophiolites, *in* Malpas, J., et al., eds., Ophiolites, Oceanic Crustal Analogues: Proceedings of the Symposium "Troodos 1987," Geological Survey Department, Nicosia, Cyprus, p. 295–309.

Dilek, Y., and Whitney, D.L., 2000, Cenozoic crustal evolution in central Anatolia: Extension, magmatism and landscape development: Proceedings of the Third International Conference on the Geology of the Eastern Mediterranean, September 1998, Geological Survey Department, Nicosia, Cyprus, p. 183–192.

Dilek, Y., Thy, P., Hacker, B., and Grundvig, S., 1999a, Structure and petrology of Tauride ophiolites and mafic dike intrusions (Turkey): Implications for the Neo-Tethyan ocean: Bulletin of the Geological Society of America, v. 111, no. 8, p. 1192–1216, doi: 10.1130/0016-7606(1999)111<1192:SAPOTO>2.3.CO;2.

Dilek, Y., Whitney, D.L., and Tekeli, O., 1999b, Links between tectonic processes and landscape morphology in an Alpine collision zone, South-Central Turkey: Annals of Geomorphology (Z. Geomorph. N.F.), vol. 118, p. 147–164.

Dora, O.Ö., Savasçin, M.Y., Kun, N., and Candan, O., 1987, Post-metamorphic plutons in the Menderes Massif: Hacettepe University Yerbilimleri, v. 14, p. 79–89.

England, P., and Houseman, G., 1989, Extension during continental convergence, with application to Tibetan Plateau: Journal of Geophysical Research, v. 94, no. B12, p. 17,561–17,579.

Ercan, T., Türkecan, A., Akyürek, B., Günay, E., Çevikbas, A., Ates, M., Can, B., Erkan, M., and Ozkirisçi, M., 1984, Dikili-Bergama-Çandarli (Bati Anadolu) yöresinin jeolojisi ve magmatik kayaclarin petrolojisi: Jeoloji Mühendisligi Dergisi, v. 20, p. 47–60.

Ercan, T., Satir, M., Kreuzer, H., Türkecan, A., Günay, E., Çevikbas, A., Ates, M., and Can, B., 1985, Bati Anadolu Senozoyik volkanitlerine ait yeni kimyasal, izotopik ve radyometrik verilerin yorumu: Bulletin of the Geological Society of Turkey, v. 28, p. 121–136.

Ercan, T., Ergul, E., Akcoren, F., Cetin, A., Granit, S., and Asutay, J., 1990, Balikesir-Bandirma arasinin jeolojisi, Tersiyer volkanizmasinin petrolojisi ve bolgesel yayilimi: MTA Dergisi, v. 110, p. 113–130.

Ercan, T., Satir, M., Steinitz, G., Dora, A., Sarifakioglu, E., Adis, C., Walter, H.-J., and Yildirim, T., 1995, Biga yarimadasi ile Gokceada, Bozcaada ve Tavsan adalarindaki (KB Anadolu) Tersiyer volkanizmasinin ozellikleri: MTA Dergisi, v. 117, p. 55–86.

Frey, F.A., Green, D.H., and Roy, S.D., 1978, Integrated models of basalt petrogenesis: A study of Quartz tholeiite to olivine melililites from south eastern Australia utilizing geochemical and experimental data: Journal of Petrology, v. 19, p. 463–513.

Fytikas, M., Innocenti, F., Manetti, P., Mazzuoli, R., Peccerillo, A., and Villari, L., 1984, Tertiary to Quaternary evolution of volcanism in the Aegean region, *in* Dixon, J.E., and Robertson, A.H.F., eds., The geological evolution of the Eastern Mediterranean: Geological Society of London Special Publication 17, p. 687–700.

Genç, S.C., 1998, Evolution of the Bayramiç magmatic complex, northwestern Anatolia: Journal of Volcanology and Geothermal Research, v. 85, no. 1–4, p. 233–249, doi: 10.1016/S0377-0273(98)00057-2.

Genç, S.C., and Yılmaz, Y., 1997, An example of post-collisional magmatim in northwestern Anatolia: the Kizderbent Volcanics (Armutlu Peninsula, Turkey): Turkish Journal of Earth Sciences, v. 6, p. 33–42.

Gerya, T.V., Yuen, D.A., and Maresch, W.V., 2004, Thermomechanical modeling of slab detachment: Earth and Planetary Science Letters, v. 226, p. 101–116, doi: 10.1016/j.epsl.2004.07.022.

Gessner, K., Collins, A.S., Ring, U., and Güngör, T., 2004, Structural and thermal history of poly-orogenic basement: U-Pb geochronology of granitoid rocks in the southern Menderes Massif, western Turkey: Journal of the Geological Society of London, v. 161, p. 93–101.

Gill, J.B., 1981, Orogenic andesites and plate tectonics: Berlin, Heidelberg, and London, Springer, 390 p.

Güleç, N., 1991, Crust-mantle interaction in western Turkey: Implications from Sr and Nd isotope geochemistry of Tertiary and Quaternary volcanics: Geological Magazine, v. 23, p. 417–435.

Gülen, L., 1990, Isotopic characterization of Aegean magmatism and geodynamic evolution of Aegean subduction, *in* Savasçin, M.Y., and Eronat, A.H., eds., International Earth Science Colloquium on the Aegean Region (IESCA), Izmir, Turkey, Proceedings, v. 2, p. 143–166.

Hansmann, W., and Oberli, F., 1991, Zircon inheritance in an igneous rock suite from the southern Adamello batholith (Italian Alps): Implications for petrogenesis: Contributions to Mineralogy and Petrology, v. 107, p. 501–518, doi: 10.1007/BF00310684.

Harris, N.B.W., Kelley, S., and Okay, A.I., 1994, Post-collisional magmatism and tectonics in northwest Anatolia: Contributions to Mineralogy and Petrology, v. 117, p. 241–252, doi: 10.1007/BF00310866.

Hart, S.R., and Davis, K.E., 1978, Nickel partitioning between olivine and silicate melt: Earth and Planetary Science Letters, v. 40, p. 203–219, doi: 10.1016/0012-821X(78)90091-2.

Hawkesworth, C.J., Gallagher, K., Hergt, J.M., and McDermott, F., 1993, Mantle and slab contributions in arc magmas: Annual Review of Earth and Planetary Sciences, v. 21, p. 175–204.

Hetzel, R., and Reischmann, T., 1996, Intrusion age of Pan-African augen gneisses in the southern Menderes Massif and the age of cooling after Alpine ductile extensional deformation: Geological Magazine, v. 133, p. 565–572.

Houseman, G.A., McKenzie, D.P., and Molnar, P., 1981, Convective instability of a thickened boundary layer and its relevance for the thermal evolution of continental convergent belts: Journal of Geophysical Research, v. 86, no. B7, p. 6115–6132.

Inci, U., 1998, Miocene synvolcanic alluvial sedimentation in ignimbrite-bearing Soma Basin, western Turkey: Turkish Journal of Earth Sciences, v. 7, p. 63–78.

Irvine, T.N., and Baragar, W.R.A., 1971, A guide to the chemical classification of common volcanic rocks: Canadian Journal of Earth Sciences, v. 8, p. 523–548.

Jackson, J., and McKenzie, D., 1988, Rates of active deformation in the Aegean Sea and surrounding areas: Basin Research, v. 1, p. 121–128.

Jolivet, L., Brun, J.P., Gautier, S., Lallemand, S., and Patriat, M., 1994a, 3-D kinematics of extension in the Aegean from the early Miocene to the present: Insight from the ductile crust: Bulletin de la Société Géologique de France, v. 165, p. 195–209.

Jolivet, L., Daniel, J.M., Truffert, C., and Goffé, B., 1994b, Exhumation of deep-crustal metamorphic rocks and crustal extension in arc and back-arc regions: Lithos, v. 33, p. 3–30, doi: 10.1016/0024-4937(94)90051-5.

Juteau, T., 1980, Ophiolites of Turkey: Ofioliti, v. 2, p. 199–238.

Karacik, Z., and Yılmaz, Y., 1998, Geology of the ignimbrites and the associated volcano-plutonic complex of the Ezine area, northwestern Anatolia: Journal of Volcanology and Geothermal Research, v. 85, p. 251–264, doi: 10.1016/S0377-0273(98)00058-4.

Keller, J., 1983, Potassic volcanism of the Mediterranean area: Journal of Volcanology and Geothermal Research, v. 18, p. 321–335, doi: 10.1016/0377-0273(83)90014-8.

Keskin, M., 2003, Magma generation by slab steepening and breakoff beneath a subduction-accretion complex: An alternative model for collision-related volcanism in eastern Anatolia, Turkey: Geophysical Research letters, v. 30, no. 24, p. 8046, doi: 10.1029/2003GL018019.

Ketin, I., 1948, Über die tektonisch-mechanischen Folgerungen aus den grossen anatolischen Erdbeben des letzten Dezenniums: Geologische Rundschau, v. 36, p. 77–83, doi: 10.1007/BF01791916.

Köprübasi, N., and Aldanmaz, E., 2004, Geochemical constraints on the petrogenesis of Cenozoic I-type granitoids in Northwest Anatolia, Turkey: Evidence for magma generation by lithospheric delamination in a post-collisional setting: International Geology Review, v. 46, p. 705–729.

Kreemer, C., Holt, W.E., and Haines, A.J., 2003, An integrated global model of present-day plate motions and plate boundary deformation: Geophysical Journal International, v. 154, p. 8–34, doi: 10.1046/j.1365-246X.2003.01917.x.

Kuno, H., 1966, Lateral variation of basalt magma type across continental margins and island arcs: Bulletin of Volcanology, v. 29, p. 195–222.

Le Bas, M.J., Le Maitre, R.W., Streckeisen, A., and Zanettin, B., 1986, A chemical classification of volcanic rocks based on total Alcali-Silica content: Journal of Petrology, v. 27, p. 745–750.

Lenardic, A., and Kaula, W.M., 1995, More thoughts on convergent crustal plate formation and mantle dynamics with regard to Tibet: Journal of Geophysical Research, v. 100, p. 15,193–15,203, doi: 10.1029/95JB01289.

LePichon, X., and Angelier, J., 1979, The Hellenic arc and trench system: A key to the neotectonic evolution of the eastern Mediterranean area: Tectonophysics, v. 60, p. 1–42, doi: 10.1016/0040-1951(79)90131-8.

LePichon, X., Chamot-Rooke, N., Lallemant, S., Noomen, R., and Veis, G., 1995, Geodetic determination of the kinematics of central Greece with respect to Europe: Implications for eastern Mediterranean tectonics: Journal of Geophysical Research, v. 100, p. 12,675–12,690, doi: 10.1029/95JB00317.

Lister, G.S., and Forster, M., 1996, Inside the Aegean metamorphic core complexes: Technical Publications of the Australian Crustal Research Centre, v. 45, 110 p.

Marchev, P., Raicheva, R., Downes, H., Vaselli, O., Chiaradia, M., and Moritz, R., 2004, Compositional diversity of Eocene–Oligocene basaltic magmatism in the Eastern Rhodopes, SE Bulgaria: Implications for genesis and tectonic setting: Tectonophysics, v. 393, no. 1–4, p. 301–328, doi: 10.1016/j.tecto.2004.07.045.

Maury, R.C., Defant, M.J., and Joron, J.L., 1992, Metasomatism of arc mantle inferred from trace elements in Philippine xenoliths: Nature, v. 360, p. 661–663, doi: 10.1038/360661a0.

Maury, R.C., Fourcade, S., and Coulon, C., Azzouzi, M.E., Bellon, H., Coutelle, A., Ouabadi, A., Semroud, B., Megartsi, M., Cotton, J., Belanteur, O., Louni-Haccini, A., Pique, A., Capdevila, R., Hernandez, J., and Réhault, J.P., 2000, Post-collisional Neogene magmatism of the Mediterranean Maghreb margin: A consequence of slab breakoff: Earth and Planetary Sciences, v. 331, p. 159–173.

McClusky, S., Balassanian, S., Barka, A., Demir, C., Ergintav, S., Georgiev, I., Gürkan, O., Hamburger, M., Hurst, K., Kahle, H., Kastens, K., Kekelidze, G., King, R., Kotzev, V., Lenk, O., Mahmoud, S., Mishin, A., Nadariya, M., Ouzounis, A., Paradissis, D., Peter, Y., Prilepin, M., Reilinger, R., Sanli, I., Seeger, H., Tealeb, A., Toksöz, M.N., and Veis, G., 2000, GPS constraints on plate motions and deformations in the eastern Mediterranean: Implications for plate dynamics: Journal of Geophysical Research, v. 105, p. 5695–5719, doi: 10.1029/1999JB900351.

McCulloch, M.T., and Gamble, J.A., 1991, Geochemical and geodynamical constrains on subduction zone magmatism: Earth and Planetary Science Letters, v. 102, p. 358–374, doi: 10.1016/0012-821X(91)90029-H.

McDonough, W.F., 1990, Constrains on the composition of the continental lithospheric mantle: Earth and Planetary Science Letters, v. 102, p. 358–374.

McKenzie, D., 1972, Active tectonics of the Mediterranean region: Geophysical Journal of the Royal Astronomical Society, v. 30, p. 109–185.

McKenzie, D., 1978, Active tectonics of the Alpine-Himalayan belt, the Aegean Sea and surrounding regions: Geophysical Journal of the Royal Astronomical Society, v. 55, p. 217–254.

McKenzie, D., and Yılmaz, Y., 1991, Deformation and volcanism in Western Turkey and the Aegean: Bulletin of the Technical University of Istanbul, v. 44, p. 345–373.

Meulenkamp, J.E., Wortel, W.J.R., Van Wamel, W.A., Spakman, W., and Hoogerduyn, S.E., 1988, On the Hellenic subduction zone and geodynamic evolution of Crete since the late Middle Miocene: Tectonophysics, v. 146, p. 203–215, doi: 10.1016/0040-1951(88)90091-1.

Nemcok, M., Pospisil, L., Lexa, J., and Donelick, R.A., 1998, Tertiary subduction and slab break-off model of the Carpathian-Pannonian region: Tectonophysics, v. 295, p. 307–340, doi: 10.1016/S0040-1951(98)00092-4.

Okay, A.I., 1984, Distribution and characteristics of the northwest Turkish blueschists, *in* The geological evolution of the Eastern Mediterranean region: Geological Society of London Special Publication 17, p. 455–466.

Okay, A.I., 2002, Accretional and collisional orogens in Anatolia: Geological Society of America Abstracts with Programs, v. 34, no. 6, p. 329–330.

Okay, A.I., and Satir, M., 2000, Coeval plutonism and metamorphism in a latest Oligocene metamorphic core complex in northwest Turkey: Geological Magazine, v. 137, p. 495–516, doi: 10.1017/S0016756800004532.

Okay, A.I., and Satir, M., 2002, When and why did the extension start in the Aegean?: Geological Society of America Abstracts with Programs, v. 34, no. 6, p. 179.

Okay, A.I., Satir, M., Maluski, H., Siyako, M., Monie, P., Metzger, R., and Akyüz, S., 1996, Paleo- and Neo-Tethyan events in northwest Turkey: Geological and geochronological constraints, *in* Yin, A., and Harrison, M.T., eds., Tectonics of Asia: Cambridge, Cambridge University Press, p. 420–441.

Okay, A.I., Harris, N.B.W., and Kelley, S.P., 1998, Exhumation of blueschists along a Tethyan suture in northwest Turkey: Tectonophysics, v. 285, p. 275–299, doi: 10.1016/S0040-1951(97)00275-8.

Oral, B., 1994, Global Positioning System (GPS) measurements in Turkey (1988–1992): Kinematics of the Africa-Arabia-Eurasia plate collision zone [Ph.D. thesis]: MIT, Cambridge.

Özgül, N., 1984, Stratigraphy and tectonic evolution of the Central Taurides, *in* Tekeli, O., and Göncüoglu, M.C., eds., Geology of the Taurus Belt: Proceedings of the International Symposium, Geology of the Taurus Belt, Mineral Research and Exploration Institute of Turkey (MTA), Ankara, p. 77–90.

Pearce, J.A., 1982, Trace element characteristics of lavas from destructive plate boundaries, *in* Thorpe, R.S., ed., Andesites: Orogenic andesites and related rocks: Chichester, England, John Wiley & Sons, p. 525–548.

Pearce, J.A., and Peate, D.W., 1995, Tectonic implications of the composition of volcanic arc magmas: Annual Review of Earth and Planetary Sciences, v. 23, p. 251–285, doi: 10.1146/annurev.ea.23.050195.001343.

Pearce, J.A., Bender, J.F., DeLong, S.E., Kidd, W.S.F., Low, P.J., Guner, Y., Saroğlu, F., Yılmaz, Y., Moorbath, S., and Mitchell, J.J., 1990, Genesis of collision volcanism in eastern Anatolia, Turkey: Journal of Volcanology

and Geothermal Research, v. 44, p. 189–229, doi: 10.1016/0377-0273(90)90018-B.

Peccerillo, A., and Taylor, S.R., 1976, Geochemistry of Eocene calc-alkaline volcanic rocks in the Kastamonu area, Northern Turkey: Contributions to Mineralogy and Petrology, v. 58, p. 63–81, doi: 10.1007/BF00384745.

Pe-Piper, G., and Piper, D.J.W., 1989, Spatial and temporal variations in late Cenozoic back-arc volcanic rocks, Aegean Sea region: Tectonophysics, v. 169, p. 113–134, doi: 10.1016/0040-1951(89)90186-8.

Pe-Piper, G., and Piper, D.J.W., 1992, Geochemical variation with time in the Cenozoic high-K volcanic rocks of the island of Lesbos, Greece: Significance for shoshonite petrogenesis: Journal of Volcanology and Geothermal Research, v. 53, p. 371–387, doi: 10.1016/0377-0273(92)90092-R.

Pe-Piper, G., and Piper, D.J.W., 2001, Late Cenozoic, post-collisional Aegean igneous rocks: Nd, Pb, and Sr isotopic constraints on petrogenetic and tectonic models: Geological Magazine, v. 138, p. 653–668.

Richardson-Bunbury, J.M., 1996, The Kula volcanic field, western Turkey: The development of a Holocene alkali basalt province and the adjacent normal-faulting graben: Geological Magazine, v. 133, p. 275–283.

Ricou, L.E., Argyriadis, I., and Marcoux, J., 1975, L'axe calcaire du Taurus, un alignement de fenêtres arabo-africaines sous des nappes radiolaritiques, ophiolitiques et métamorphiques: Bulletin de la Société Géologique de France, v. 16, p. 107–111.

Rimmelé, G., Oberhänsli, R., Goffé, B., Jolivet, L., Candan, O., and Çetinkaplan, M., 2003, First evidence of high-pressure metamorphism in the "Cover Series" of the Southern Menderes Massif: Tectonic and metamorphic implications for the evolution of SW Turkey: Lithos, v. 71, p. 19–46, doi: 10.1016/S0024-4937(03)00089-6.

Ring, U., and Collins, A.S., 2005, U-Pb SIMS dating of synkinematic granites: Timing of core-complex formation in the northern Anatolide belt of western Turkey: Journal of the Geological Society of London, v. 162, p. 289–298, doi: 10.1144/0016-764904-016.

Ring, U., and Layer, P.W., 2003, High-pressure metamorphism in the Aegean, eastern Mediterranean: Underplating and exhumation from the Late Cretaceous until the Miocene to Recent above the retreating Hellenic subduction zone: Tectonics, v. 22, p. 6-1–6-23, doi: 10.1029/2001TC001350.

Ring, U., Johnson, C., Hetzel, R., and Gessner, K., 2003, Tectonic denudation of a Late Cretaceous–Tertiray collisional belt: Regionally symmetric cooling patterns and their relation to extensional faults in the Anatolide belt of western Turkey: Geological Magazine, v. 140, p. 421–441, doi: 10.1017/S0016756803007878.

Saunders, A.D., Norry, M.J., and Tarney, J., 1991, Fluid influence on the trace element compositions of subduction zone magmas: Philosophical Transactions of the Royal Society of London, v. A335, p. 377–392.

Savaşçin, M.Y., and Dora, Ö.O., 1979, An approach to the young magmatic evolution of western Anatolia: Fortschritte der Mineralogie, v. 57–1, nos. 1 and 2, p. 132–133.

Savaşçin, M.Y., and Güleç, N., 1990, Relationship between magmatic and tectonic activities in western Turkey, *in* Savaşçin, M.Y., and Eronat, A.H., eds., International Earth Science Colloquium on the Aegean Region (IESCA), Proceedings, II, p. 300–313.

Savaşçin, M.Y., and Erler, A., 1994, Neogene–Quaternary magmatism and related ore deposits of western Anatolia: International Volcanological Congress, IAVCEI Ankara 1994, Excursion Guidebook (A2), 56 p.

Savaşçin, M.Y., and Oyman, T., 1998, Tectono-magmatic evolution of alkaline volcanics at the Kirka-Afyon-Isparta structural trend, SW Turkey: Turkish Journal of Earth Sciences, v. 7, p. 201–214.

Schiano, P., Clocchiatti, R., Shimizu, N., Mury, R.C., Johum, K.P., and Hofmann, A.W., 1995, Hydrous, silica rich melts in the subarc mantle and their relationship with erupted arc lavas: Nature, v. 377, p. 595–600, doi: 10.1038/377595a0.

Schliestedt, M., Altherr, R., and Matthews, A., 1987, Evolution of the Cycladic Crystalline Complex: Petrology, isotope geochemistry and geochronology, *in* Helgeson, H.C., ed., Chemical transport in metasomatic processes: Dordrecht, Reidel, p. 389–428.

Seghedi, I., Downes, H., Szakács, A., Mason, P.R.D., Thirwall, M.F., Rosu, E., Pécskay, Z., Márton, E., and Panaiotu, 2004, Neogene–Quaternary magmatism and geodynamics in the Carpathian-Pannonian region: A synthesis: Lithos, v. 72, p. 117–146, doi:10.1016/j.lithos.2003.08.006.

Şengör, A.M.C., and Yılmaz, Y., 1981, Tethyan evolution of Turkey: A plate tectonic approach: Tectonophysics, v. 75, p. 181–241, doi: 10.1016/0040-1951(81)90275-4.

Şengör, A.M.C., Satir, M., and Akkök, R., 1984, Timing of tectonic events in the Menderes Massif, western Turkey: Implications for tectonic evolution and evidence for Pan-African basement in Turkey: Tectonics, v. 3, p. 693–707.

Şengör, A.M.C., Görür, N., and Saroğlu, F., 1985, Strike-slip deformation, basin formation and sedimentation: Strike-slip faulting and related basin formation in zones of tectonic escape: Turkey as a case study: Society of Economic Paleontology and Mineralogy Special Publication 37, p. 227–264.

Şengör, A.M.C., Özeren, S., Gena, T., and Zor, E., 2003, East Anatolian high plateau as a mantle-supported north-south shortened domal structure: Geophysical Research Letters, v. 30, no. 24, p. 8045, doi: 10.1029/2003GL017858.

Seyitoğlu, G., and Scott, B., 1991, Late Cenozoic crustal extension and basin formation in West Turkey: Geological Magazine, v. 128, p. 155–166.

Seyitoğlu, G., and Scott, B., 1992, Late Cenozoic volcanic evolution of the northeastern Aegean region: Journal of Volcanology and Geothermal Research, v. 54, p. 157–176, doi: 10.1016/0377-0273(92)90121-S.

Seyitoğlu, G., and Scott, B., 1996, The cause of N-S extensional tectonics in western Turkey: Tectonic escape vs. backarc spreading vs. orogenic collapse: Journal of Geodynamics, v. 22, p. 145–153, doi: 10.1016/0264-3707(96)00004-X.

Seyitoğlu, G., Anderson, D., Nowell, G., and Scott, B., 1997, The evolution from Miocene potassic to Quaternary sodic magmatism in western Turkey: Implications for enrichment processes in the lithospheric mantle: Journal of Volcanology and Geothermal Research, v. 76, p. 127–147, doi: 10.1016/S0377-0273(96)00069-8.

Sherlock, S., Kelley, S.P., Inger, S., Harris, N., and Okay, A.I., 1999, ^{40}Ar-^{39}Ar and Rb-Sr geochronology of high-pressure metamorphism and exhumation history of the Tavsanli Zone, NW Turkey: Contributions to Mineralogy and Petrology, v. 137, p. 46–58, doi: 10.1007/s004100050581.

Sun, S.S., and McDonough, W.F., 1989, Chemical and isotopic systematics of oceanic basalts: Implications for mantle composition and processes, *in* Saunders, A.D., and Norry, M.J., eds., Magmatism in the ocean basins: Geological Society of London Special Publication 42, p. 313–345.

Tankut, A., Dilek, Y., and Önen, P., 1998, Petrology and geochemistry of the Neo-Tethyan volcanism as revealed in the Ankara Melange, Turkey: Journal of Volcanological and Geothermal Research, v. 85, p. 265–284, doi: 10.1016/S0377-0273(98)00059-6.

Taymaz, T., Jackson, J., and McKenzie, D., 1991, Active tectonics of the north and central Aegean Sea: Geophysical Journal International, v. 106, p. 433–490.

Tekeli, O., 1981, Subduction complex of pre-Jurassic age, northern Anatolia, Turkey: Geology, v. 9, p. 68–72, doi: 10.1130/0091-7613(1981)9<68:SCOPAN>2.0.CO;2.

Thirlwall, M.F., Smith, T.E., Graham, A.M., Theodorou, N., Hollings, P., Davidson, J.P., and Arculus, R.D., 1994, High field strength element anomalies in arc lavas: Source or processes: Journal of Petrology, v. 35, p. 819–838.

Thorpe, R.S., Francis, P.W., Hammill, M., and Baker, M.C.W., 1982, The Andes, *in* Thorpe, R.S., ed., Andesites: Orogenic andesites and related rocks: Chichester, England, John Wiley & Sons, p. 187–205.

Turner, S., Arnaud, N., Liu, J., Rogers, N., Hawkesworth, C., Harris, N., Kelley, S., Calsteren, P.V., and Deng, W., 1996, Post collision, shoshonitic volcanism on the Tibetan Plateau: Implications for convective thinning of the lithosphere and the source of Ocean Island Basalts: Journal of Petrology, v. 37, p. 45–71.

Walker, J.A., Moulds, T.N., Zentilli, M., and Feigeson, M.D., 1991, Spatial and temporal variations in volcanics of Andean central volcanic zone (26 to 28),

in Harmon, R.S., and Rapela, C.W., eds., Andean magmatism and its tectonic setting: Geological Society of America Special Paper 265, p. 139–155.

Williams, H.M., Turner, S.P., Pearce, J.A., Kelley, S.P., and Harris, N.B.W., 2004, Nature of the source regions for post-collisional, potassic magmatism in southern and northern Tibet from geochemical variations and inverse trace element modelling: Journal of Petrology, v. 45, no. 3, p. 555–607, doi: 10.1093/petrology/egg094.

Wortel, M.J.R., and Spakman, W., 2000, Subduction and slab detachment in the Mediterranean-Carpathian region: Science, v. 290, p. 1910–1917, doi: 10.1126/science.290.5498.1910.

Yılmaz, K., 1992, Mekece (Adapazari)–Bahçekik (Kocaeli) dolayının jeolojik ve petrolojik incelemesi [Ph.D. thesis]: Istanbul Üniversitesi Fen Bilimleri Enstitüsü, 260 p.

Yılmaz, Y., 1989, An approach to the origin of young volcanic rocks of western Turkey, *in* Şengör, A.M.C., ed., Tectonic evolution of the Tethyan region: The Hague, Kluwer, p. 159–189.

Yılmaz, Y., 1990, Comparison of young volcanic associations of western and eastern Anatolia under compressional regime: A review: Journal of Volcanology and Geothermal Research, v. 44, p. 69–87, doi: 10.1016/0377-0273(90)90012-5.

Yılmaz, Y., 1997, Geology of western Anatolia: Active Tectonics of northwestern Anatolia: The Marmara Poly-Project, a multi disciplinary approach by space-geodesy, geology, hydrogeology, geothermics and seismology: Zurich, Vdf Hochschulverlag AG an der ETH, p. 31–53.

Yılmaz, Y., 2002, Tectonic evolution of western Anatolian extensional province during the Neogene and Quaternary: Geological Society of America Abstracts with Programs, v. 34, no. 6, p. 179.

Yılmaz, Y., and Polat, A., 1998, Geology and evolution of the Thrace volcanism, Turkey: Acta Vulcanologica, v. 10, p. 293–303.

Yılmaz, Y., Genç, S.C., Gürer, O.F., Bozcu, M., Yılmaz, K., Karacik, Z., Altunkaynak, Ş., and Elmas, A., 2000, When did the western Anatolian grabens begin to develop?, *in* Bozkurt, E., et al., eds., Tectonics and magmatism in Turkey and the surrounding area: Geological Society of London Special Publication 173, p. 353–384.

Yılmaz, Y., Genç, S.C., Karacik, Z., and Altunkaynak, Ş., 2001, Two contrasting magmatic associations of NW Anatolia and their tectonic significance: Journal of Geodynamics, v. 31, p. 243–271, doi: 10.1016/S0264-3707(01)00002-3.

Manuscript Accepted by the Society 30 December 2005

Printed in the USA